IAEA
International Atomic Energy Agency

Passive Autocatalytic Recombiner Part-Task Simulator

Manual and Practical Exercises

VIENNA, 2023

TRAINING COURSE SERIES 80

PASSIVE AUTOCATALYTIC RECOMBINER PART-TASK SIMULATOR

The following States are Members of the International Atomic Energy Agency:

AFGHANISTAN
ALBANIA
ALGERIA
ANGOLA
ANTIGUA AND BARBUDA
ARGENTINA
ARMENIA
AUSTRALIA
AUSTRIA
AZERBAIJAN
BAHAMAS
BAHRAIN
BANGLADESH
BARBADOS
BELARUS
BELGIUM
BELIZE
BENIN
BOLIVIA, PLURINATIONAL STATE OF
BOSNIA AND HERZEGOVINA
BOTSWANA
BRAZIL
BRUNEI DARUSSALAM
BULGARIA
BURKINA FASO
BURUNDI
CABO VERDE
CAMBODIA
CAMEROON
CANADA
CENTRAL AFRICAN REPUBLIC
CHAD
CHILE
CHINA
COLOMBIA
COMOROS
CONGO
COSTA RICA
CÔTE D'IVOIRE
CROATIA
CUBA
CYPRUS
CZECH REPUBLIC
DEMOCRATIC REPUBLIC OF THE CONGO
DENMARK
DJIBOUTI
DOMINICA
DOMINICAN REPUBLIC
ECUADOR
EGYPT
EL SALVADOR
ERITREA
ESTONIA
ESWATINI
ETHIOPIA
FIJI
FINLAND
FRANCE
GABON
GAMBIA
GEORGIA
GERMANY
GHANA
GREECE
GRENADA
GUATEMALA
GUYANA
HAITI
HOLY SEE
HONDURAS
HUNGARY
ICELAND
INDIA
INDONESIA
IRAN, ISLAMIC REPUBLIC OF
IRAQ
IRELAND
ISRAEL
ITALY
JAMAICA
JAPAN
JORDAN
KAZAKHSTAN
KENYA
KOREA, REPUBLIC OF
KUWAIT
KYRGYZSTAN
LAO PEOPLE'S DEMOCRATIC REPUBLIC
LATVIA
LEBANON
LESOTHO
LIBERIA
LIBYA
LIECHTENSTEIN
LITHUANIA
LUXEMBOURG
MADAGASCAR
MALAWI
MALAYSIA
MALI
MALTA
MARSHALL ISLANDS
MAURITANIA
MAURITIUS
MEXICO
MONACO
MONGOLIA
MONTENEGRO
MOROCCO
MOZAMBIQUE
MYANMAR
NAMIBIA
NEPAL
NETHERLANDS
NEW ZEALAND
NICARAGUA
NIGER
NIGERIA
NORTH MACEDONIA
NORWAY
OMAN
PAKISTAN
PALAU
PANAMA
PAPUA NEW GUINEA
PARAGUAY
PERU
PHILIPPINES
POLAND
PORTUGAL
QATAR
REPUBLIC OF MOLDOVA
ROMANIA
RUSSIAN FEDERATION
RWANDA
SAINT KITTS AND NEVIS
SAINT LUCIA
SAINT VINCENT AND THE GRENADINES
SAMOA
SAN MARINO
SAUDI ARABIA
SENEGAL
SERBIA
SEYCHELLES
SIERRA LEONE
SINGAPORE
SLOVAKIA
SLOVENIA
SOUTH AFRICA
SPAIN
SRI LANKA
SUDAN
SWEDEN
SWITZERLAND
SYRIAN ARAB REPUBLIC
TAJIKISTAN
THAILAND
TOGO
TONGA
TRINIDAD AND TOBAGO
TUNISIA
TÜRKİYE
TURKMENISTAN
UGANDA
UKRAINE
UNITED ARAB EMIRATES
UNITED KINGDOM OF GREAT BRITAIN AND NORTHERN IRELAND
UNITED REPUBLIC OF TANZANIA
UNITED STATES OF AMERICA
URUGUAY
UZBEKISTAN
VANUATU
VENEZUELA, BOLIVARIAN REPUBLIC OF
VIET NAM
YEMEN
ZAMBIA
ZIMBABWE

The Agency's Statute was approved on 23 October 1956 by the Conference on the Statute of the IAEA held at United Nations Headquarters, New York; it entered into force on 29 July 1957. The Headquarters of the Agency are situated in Vienna. Its principal objective is "to accelerate and enlarge the contribution of atomic energy to peace, health and prosperity throughout the world''.

TRAINING COURSE SERIES No. 80

PASSIVE AUTOCATALYTIC RECOMBINER PART-TASK SIMULATOR

MANUAL AND PRACTICAL EXERCISES

INTERNATIONAL ATOMIC ENERGY AGENCY
VIENNA, 2023

COPYRIGHT NOTICE

For further information on this publication, please contact:

Nuclear Power Technology Development Section
International Atomic Energy Agency
Vienna International Centre
PO Box 100
1400 Vienna, Austria
Email: Official.Mail@iaea.org

PASSIVE AUTOCATALYTIC RECOMBINER PART-TASK SIMULATOR: MANUAL AND PRACTICAL EXERCISES
IAEA, VIENNA, 2023
IAEA-TCS-80
ISSN 1018–5518

Printed by the IAEA in Austria
November 2023

FOREWORD

The IAEA offers its Member States a wide spectrum of education and training activities. These include face-to-face training courses and workshops, on-line learning, fellowship programmes and schools, as well as publications in the IAEA's Training Course Series, including handbooks, textbooks and manuals on various nuclear related topics.

Experience shows that education and training supported by hands-on learning by doing using nuclear power plant simulators is an effective way for a broad range of target groups to meet education and training standards. The IAEA regularly publishes reference material and holds training courses to assist professionals in Member States in understanding nuclear power plant simulators and associated technologies. The education and training courses support an integrated approach that combines lectures with learning by doing on the specifics of plant operation, including reactor physics, thermal hydraulics and safety aspects, using basic principle simulators.

Classification, Selection and Use of Nuclear Power Plant Simulators for Education and Training (IAEA-TECDOC-1887) provides information for educational institutions, training centres and suppliers on the proper classification, selection and use of various types of nuclear power plant simulators. The IAEA also provides opportunities for hands-on learning using nuclear reactor simulation computer programs, either full plant basic principle simulators or part-task simulators addressing specific parts of plant operations (i.e. systems or components) or specific phenomena. The simplified reactor designs of basic principle simulators allow professionals to grasp fundamental concepts without becoming overwhelmed by the details of a more complex, full scope simulator. The objective of these basic principle full plant or part-task simulators is to provide insight into and a practical understanding of the operational characteristics of reactors as well as plant responses to perturbations and accident scenarios. Access to both types of basic principle simulator is available to Member States upon request, and thus represents a valuable resource for teaching and training on a wide range of topics relevant to nuclear power plant design, safety, technology, simulation and operations.

This publication provides a comprehensive explanation of the passive autocatalytic recombiner part-task simulator as well as practical exercises to help readers become familiar with its use. By engaging in these exercises with the part-task simulator, readers will gain hands-on experience and a deeper understanding of its workings.

The IAEA officer responsible for this publication was T. Jevremovic of the Division of Nuclear Power.

EDITORIAL NOTE

This publication has been prepared from the original material as submitted by the contributors and has not been edited by the editorial staff of the IAEA. The views expressed remain the responsibility of the contributors and do not necessarily reflect those of the IAEA or the governments of its Member States.

Guidance and recommendations provided here in relation to identified good practices represent expert opinion but are not made on the basis of a consensus of all Member States.

Neither the IAEA nor its Member States assume any responsibility for consequences which may arise from the use of this publication. This publication does not address questions of responsibility, legal or otherwise, for acts or omissions on the part of any person.

The use of particular designations of countries or territories does not imply any judgement by the publisher, the IAEA, as to the legal status of such countries or territories, of their authorities and institutions or of the delimitation of their boundaries.

The mention of names of specific companies or products (whether or not indicated as registered) does not imply any intention to infringe proprietary rights, nor should it be construed as an endorsement or recommendation on the part of the IAEA.

The authors are responsible for having obtained the necessary permission for the IAEA to reproduce, translate or use material from sources already protected by copyrights.

The IAEA has no responsibility for the persistence or accuracy of URLs for external or third party Internet web sites referred to in this publication and does not guarantee that any content on such web sites is, or will remain, accurate or appropriate.

CONTENTS

1. INTRODUCTION

1.1. BACKGROUND

In support of human resource development in Member States, the IAEA has established education and training programmes on active learning about nuclear technologies using basic principle nuclear power plant and part-task simulators. As part of this programme, the IAEA arranges for the development and distribution of its suites of basic principle simulators including the manuals and related documentation, supports education and training courses and workshops on physics and technology of advanced reactors, methodology on technology assessment and technology relevant databases.

Hands-on learning using nuclear power plant simulators has become an essential tool for education and training programmes worldwide. Experience shows that simulators are effective in allowing a broad range of target groups to meet education and training standards. The International Atomic Energy Agency (IAEA) has been at the forefront of promoting and supporting the use of simulators for education and training purposes. The IAEA TECDOC-1887 on Classification, Selection and Use of Nuclear Power Plant Simulators for Education and Training provides guidance for educational institutions, training centres, and suppliers on the proper classification, selection, and use of various types of simulators [1]. The IAEA assists Member States by providing education and training courses on the physics and technology of nuclear power plant operation through hands-on learning with nuclear reactor simulation computer programs. The programs may refer to full plant basic principle simulators or to part-task simulators addressing specific parts of plant operations (systems or components) or specific phenomena. Both types of basic principle simulators are available to Member States upon request, representing an accessible resource for teaching and training on a wide range of topics relevant to nuclear power plant design, safety, technology, simulation, and operations. The basic principle simulators available through the IAEA often feature simplified reactor designs, allowing professionals to grasp fundamental concepts without becoming overwhelmed by the details of a more complex, full-scope simulator. The objective of these simulators is to provide insight into and a practical understanding of reactor operational characteristics and plant responses to transient and accident scenarios. This type of learning is critical for nuclear power plant personnel, who must be trained to respond quickly and appropriately in transient and accidental conditions. The IAEA regularly publishes reference material and holds education and training courses to assist professionals in Member States in understanding simulators and associated technologies. Education and training courses support an integrated approach that combines lectures with learning by doing on the specifics of plant operation, including reactor physics, thermal hydraulics, and safety aspects, using basic principle simulators.

This publication provides description relevant to understanding basic principles of passive autocatalytic recombiner (PAR) configuration, purpose and working, and mathematical models. Detailed description of PAR part-tasks simulator is provided together with the exercises applicable to education and training courses and workshops, or self-learning.

1.2. OBJECTIVE

The objectives of this publication are to:

- Serve as a reference for lectures on basic principles of PAR configuration, purpose and operation;
- Support Member States intending to use IAEA part-tasks simulators in national education and training programmes with a resource for necessary background information on theory of PAR operation;
- Serve as a reference for students and trainees, who may be unfamiliar with reactor operation in accident conditions and the role of PARs and thus to understand relevant theory and mathematical models at a basic principle level;
- Provide exercises for use in education and training courses, use by Member State institutions, or direct use by students or trainees.

1.3. SCOPE

The scope of this publication is to explain the underlying phenomena, modelling methodology, and application of PARs. Explanations and examples are limited to light water reactors. Other similar publications address different types of part-tasks simulators. Following an overview of PAR configuration and operation, this publication provides explanations about the part-task simulator and examples to study.

1.4. STRUCTURE

This publication contains the following descriptions:

- **Passive Autocatalytic Recombiner (Section 2)** provides an overview of PAR general purpose and designs, such as the basic configuration and functions;
- **General Instructions (Section 3)** regarding PAR part-task simulator including its configuration, modelled systems, and installation;
- **Examples (Section 4)** containing practical exercises with explanations of parameter trends and discussions on the outputs;
- **Validation and Verification of PAR Models (Section 5)** provides comparison of PAR part-task simulator results with publicly accessed literature.

2. PASSIVE AUTOCATALYTIC RECOMBINER

2.1. HISTORICAL BACKGROUND

Combustible gases, particularly hydrogen, have long been recognized as a safety concern in water cooled reactors. Combustible gases and combustion processes can pose a threat to a nuclear power plant (NPP) containment integrity. Maintaining containment integrity is of fundamental importance during the accident conditions to avoid the release of fission products into the environment. Relevant safety regulations were developed at the national and

international levels, and the guidelines and mitigation measures are adopted in NPPs worldwide. Since the accident at the Fukushima Daiichi NPP where explosions of combustible gases damaged the reactor buildings of Units 1, 3 and 4, the behaviour of combustible gases and related accident management measures, as well as measures to limit release of fission products into the environment, received great attention amid calls for further studies and analyses. The post-Fukushima Daiichi NPP accident action plans from regulatory bodies of several countries included directives to consider implementing the safety measures, such as PARs or other hydrogen mitigation measures and filtered containment venting systems as severe accident mitigation measures. Therefore, to avoid high intensity combustion risk, installation of PARs, preclusion of vent interconnectivity in case of multi-unit NPPs and monitoring of hydrogen release rates and hydrogen concentration were identified as some of the potential measures for preservation of NPPs containment integrity. Dedicated research and development programmes are ongoing at national and international levels with the objective to improve the understanding of phenomena associated with distribution, mitigation and combustion hazards and to address the issues highlighted after the Fukushima Daiichi events, such as explosion hazard in venting systems and the potential flammable mixture migration into spaces beyond the primary containment [2].

The role of a PAR in an NPP post-accident containment condition is to limit the concentration of combustible gases. Therefore, the PAR represents a passive hydrogen removal device designed to avoid formation of an explosive gas mixture. The PAR typically consists of an open-ended stainless-steel box with catalyst coated elements inside. The catalyst role is to convert (recombine) hydrogen and oxygen into water vapour and release the heat at the catalyst surface (more detailed explanations are provided in the following sections). This generated heat as a product of recombination reaction between gases within the PAR creates a natural convective flow [3] that eliminates the needs for installing pumps or fans to transport hydrogen to the catalyst surfaces, in this making the PAR configuration simplified and easy to maintain. In addition, the PAR is self-starting device when there is hydrogen present and thus it does not require operator action.

2.2. PROMINENT CHARACTERISTICS OF PASSIVE AUTOCATALYTIC RECOMBINERS WITHIN THE PART-TASK SIMULATOR

Two mathematical models are available to study the PAR's basic principles of operation: black-box model and inmost model. Both models introduce certain assumptions but preserving the truthiness of the chemical and physical processes involved. The main assumption is that the gas is composed of hydrogen, oxygen, nitrogen, and water vapour (steam) and that this gas mixture obeys the ideal gas law. The black-box PAR model is simpler than the inmost PAR model.

2.2.1. Black-box model

The black-box PAR model assumes simplified PAR as shown in FIG. 1; the PAR is located in a confined space (representing the NPP containment) with predefined concentration of hydrogen. The black box means that the PAR is modelled based on a simplified hydrogen

recombination rate equation, which is a function of hydrogen concentration and catalyst temperature, only.

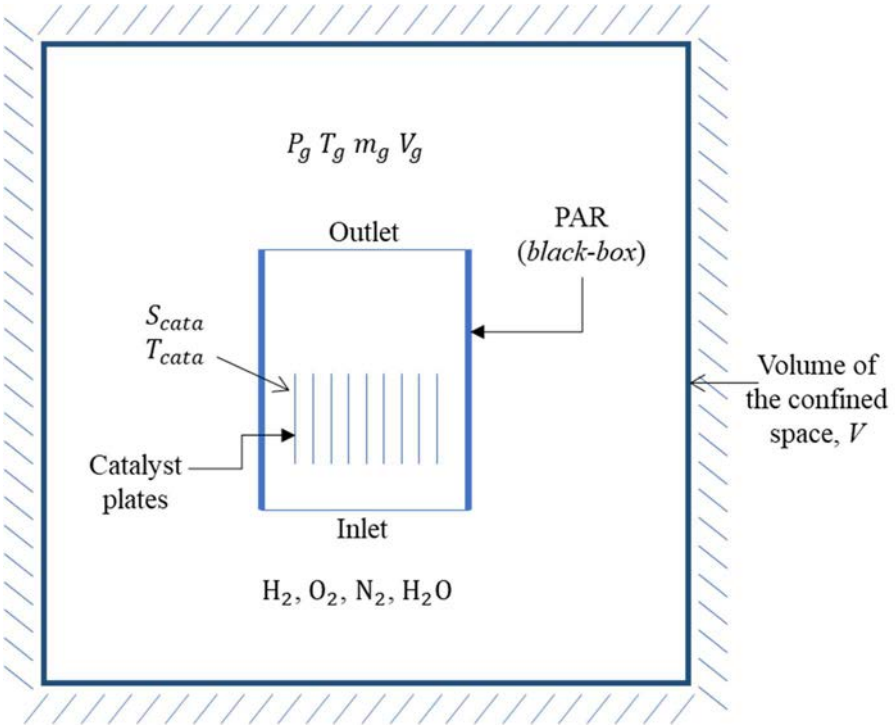

FIG. 1. Configuration and layout of the PAR black-box model.

The basic assumptions introduced to define the black-box PAR model are:

— Catalyst temperature as a function of time is pre-defined and constant along the PAR length and with respect to time;
— Confined space (representing simplified post-accident containment space) wall is adiabatic.

Hydrogen recombination at the catalyst surface is described with the chemical reaction:

$$2H_2 + O_2 \rightarrow 2H_2O + 120\ \text{kJ/g}(H_2) \tag{1}$$

The enthalpy of hydrogen combustion is 120 kJ/g(H_2). The reaction rate is described by Schefer's simple model, which assumes the first order kinetics, as follows [4]:

$$R_{rec,H_2} = 2 \cdot R_{rec,O_2} = -R_{rec,H_2O} = B \cdot \exp\left(-\frac{E}{RT_{cata}}\right) C_{H_2,cata} \tag{2}$$

where:

R_{rec} [mol/ (s·m^2)]: reaction rate of a gas at the catalyst surface;
B: pre-exponential factor which is 14 m/s;
E: reaction activation energy (14.9×10^3 J/mol);
T_{cata} [K]: catalyst temperature;

R is the universal gas constant (8.314 J/mol·K);
$C_{H_2,cata}$ [mol/m^3]: molar concentration of hydrogen at the catalyst surface;
$C_{H_2,cata}$ is approximated with:

$$C_{H_2,cata} = c_r \cdot C_{H_2} \tag{3}$$

where:

C_{H_2} [mol/m^3]: molar concentration of hydrogen in the bulk flow inside PAR;
c_r: recombination coefficient.

To approximate gas diffusion and to account for reduction in the reaction rate due to diffusion effects, this coefficient is introduced in the model as a ratio of hydrogen concentration at the catalyst surface to the freestream hydrogen concentration. Hydrogen concentration at the catalyst surface is significantly lower than the bulk hydrogen concentration. According to Schefer [4] the ratio of hydrogen concentration at the catalyst surface to the freestream concentration in the range is 0.09–0.001 (which depends on the location at the catalyst plate).

The mass balance of the x^{th} gas component is defined with:

$$\frac{dn_x}{dt} = -R_{rec,x} S_{cata} \tag{4}$$

where:

n_x [mol]: quantity of the x^{th} gas component;
S_{cata} [m^2]: active surface area of all catalyst plates collectively.

The energy balance of the gas mixture is then defined with:

$$m_g c_{v,g} \frac{dT_g}{dt} = \Delta H \cdot R_{rec,H_2} S_{cata} \tag{5}$$

where:

m_g [kg]: mass of gas;
$c_{v,g}$ [J/ (kg·K)]: gas specific heat capacity at constant volume;
T_g [K]: gas temperature;
ΔH [J/mol]: enthalpy of recombination reaction.

The specific heat capacity of a gas is calculated as a function of its temperature [5]:

$$c_v(T) = C_1 + C_2 T + C_3 T^2 + C_4 T^3 - R_{specific} \tag{6}$$

where C_1, C_2, C_3, and C_4 are polynomial constants for a gas and $R_{specific}$ [J/(kg K)] is the corresponding mass-specific gas constant. This polynomial is only valid for 273K < T < 1,800K.

The pressure of a gas mixture is obtained based on the assumption that it follows the ideal gas law:

$$P_g = \frac{n_g \times R \times T_g}{V_g} \tag{7}$$

where P_g [Pa] is gas pressure and V_g [m^3] is gas volume in the confined space.

2.2.2. Inmost model

During severe accidents in light water cooled reactors, hydrogen entering the containment is generated from various in-vessel and ex-vessel sources. The catalyst temperature changes with time and with the gas states inside and outside of the PAR. To capture these details of PAR operation, a more specific model, called the inmost PAR model, is also available within the part-task simulator. The inmost PAR configuration is shown in FIG. 2. In this model, the gas mixtures inside and outside of the PAR are considered separately: the catalyst temperature is not constant with time but determined based on the energy balance, while hydrogen is injected into a confined space at predefined rate. The reaction rate at the catalyst surface is modelled the same way as in the black-box model. Therefore, the inmost PAR model includes the following assumptions:

— Confined space wall is at constant temperature;
— PAR wall is adiabatic;
— Only convection is considered between the catalyst plates and the gas inside PAR.

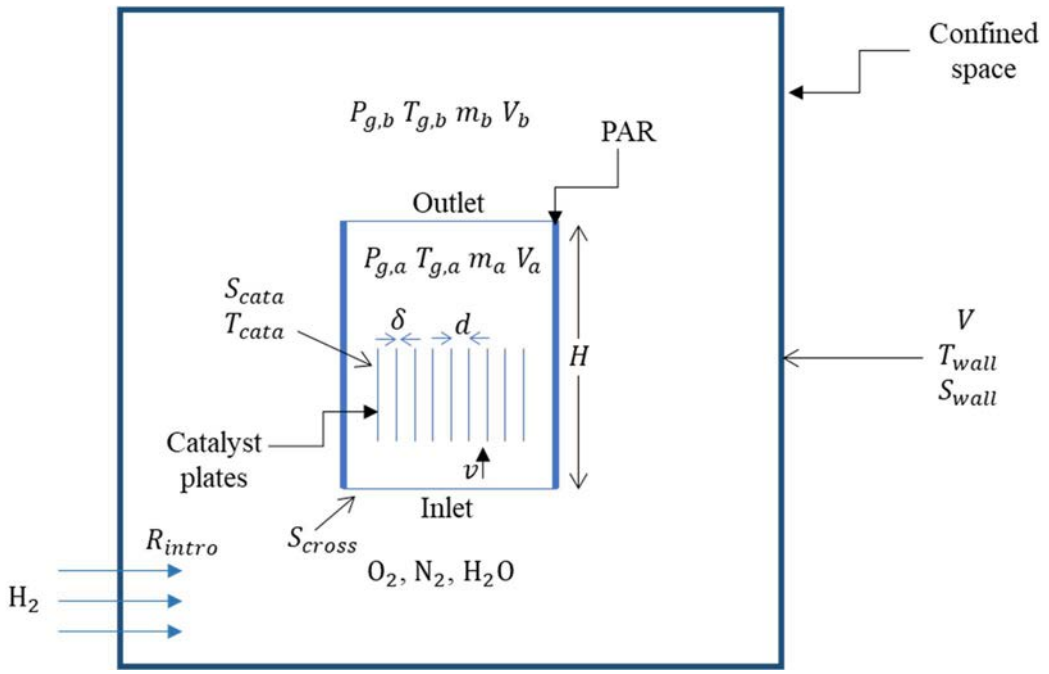

FIG. 2. Configuration and layout of the PAR inmost model.

In this model, the rate of the recombination reaction is still described with Eq. (2). The mass balance of the x^{th} gas component is now defined differently:

$$\frac{dn_{x,a}}{dt} = -R_{rec,x}S_{cata} + vS_{cross}\left(-\frac{n_{x,a}}{V_a} + \frac{n_{x,b}}{V_b}\right) \quad (9)$$

$$\frac{dn_{x,b}}{dt} = R_{intro,x} + vS_{cross}\left(\frac{n_{x,a}}{V_a} - \frac{n_{x,b}}{V_b}\right) \quad (10)$$

where $R_{intro,x}$ [mol/s] is the injection rate of the x^{th} gas component and subscripts a and b are used to denote PAR inside and outside parameters, respectively. The flow velocity v [m/s] is assumed to be constant in the PAR.

Energy generated from the recombination reaction is absorbed by the PAR's catalyst plates and the gas inside the PAR:

$$\dot{q}_{rec} = \Delta H \cdot R_{rec,H_2}S_{cata} = \dot{q}_g + \dot{q}_{cata} \quad (11)$$

where:

$\dot{q}_{rec}$ [J/s]: recombination energy generation rate;
$\dot{q}_g$ [J/s]: heat transfer rate from catalyst plates to the inside gas;
$\dot{q}_{cata}$ [J/s]: heat absorption rate of catalyst plates;
$\dot{q}_g$ and $\dot{q}_{cata}$: defined as follows:

$$\dot{q}_g = h_{cata}S_{cata}(T_{cata} - T_{g,a}) \quad (12)$$

$$\dot{q}_{cata} = m_{cata}c_{p,cata}\frac{dT_{cata}}{dt} \quad (13)$$

where h_{cata} [W/ (m^2 K)] is the heat transfer coefficient between the catalyst plates and the gas inside the PAR. The heat is transferred by natural convection flow from the catalyst plates to the gas inside the PAR. It is also abetted by forced convection due to chimney effect of the PAR structure. Hence, a realistic heat transfer coefficient calculation would require a complex model to account for these effects. In addition, the flow velocity inside the PAR varies along its length, which results in different flow regimes [6]. Given the main purpose of this model is to develop a part-task simulator for educational purpose, the flow velocity and heat transfer coefficient is set to constant value.

As shown in FIG. 3 an iterative calculation scheme is used to obtain the energy distribution between catalyst plates and the gas inside the PAR. Firstly, the catalyst temperature is calculated assuming that the energy is moved into catalyst plates. Based on the Eq. (12), the energy transfer to the gas inside of the PAR is obtained. In the next step, the energy transfer to catalyst and the catalyst temperature are updated based on the Eq. (11). The calculation is converted when the difference between the two consecutive catalyst temperatures is less than 0.5 K.

The following relation describes the energy balance for the gas inside the PAR based on the energy exchange with the gas outside of PAR and the catalyst plates:

$$m_a c_{v,a} \frac{dT_{g,a}}{dt} = \dot{q}_g - \dot{m}_{out} c_{v,a} T_{g,a} + \dot{m}_{in} c_{v,b} T_{g,b} \quad (14)$$

where $\dot{m}_{out}$ [kg/s] and $\dot{m}_{in}$ [kg/s] are the mass flow rates at PAR outlet and inlet, respectively.

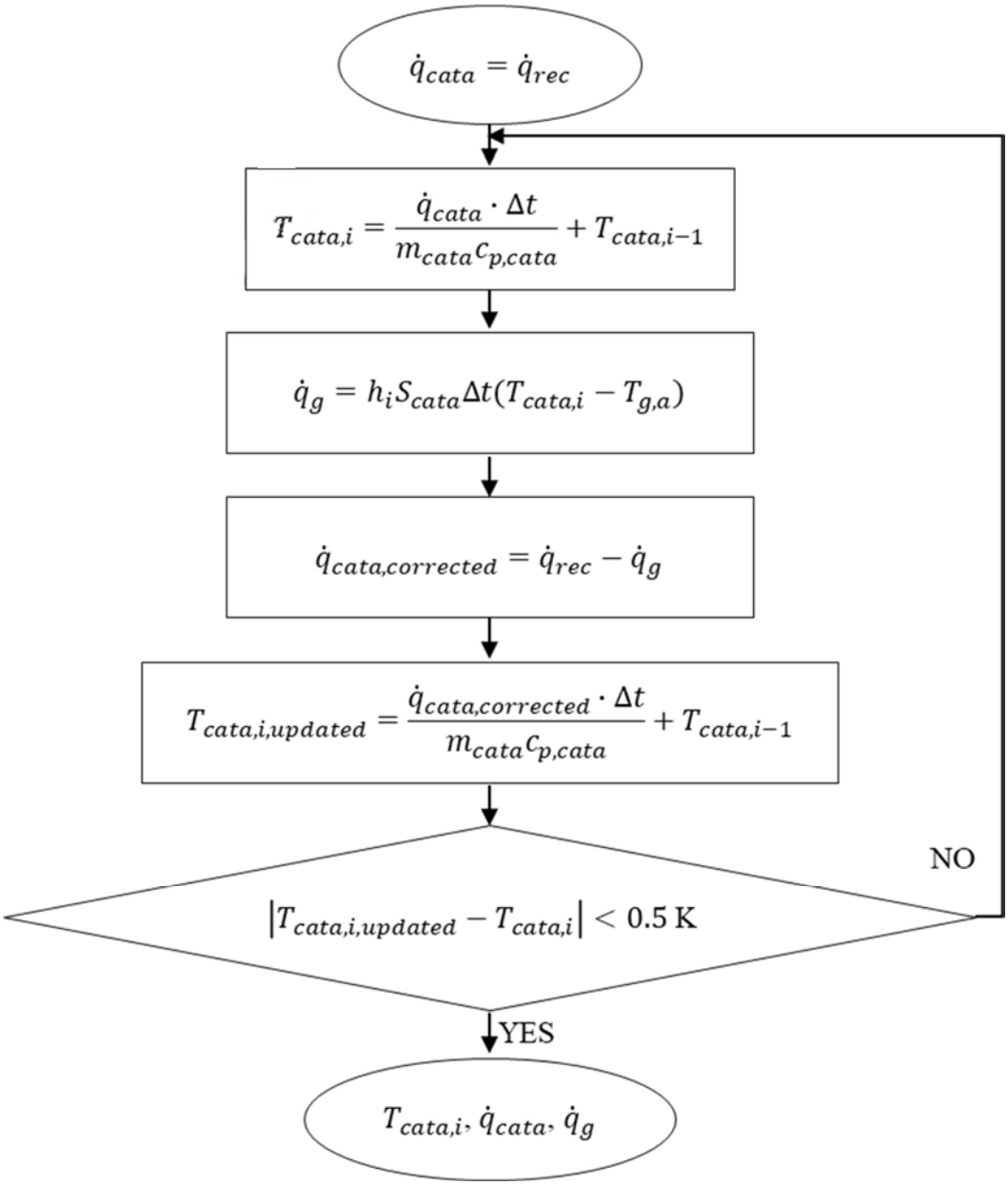

FIG. 3. Inmost PAR model iterative calculation of heat distribution between catalyst plates and the gas inside PAR, and catalyst plates temperature.

The energy balance for the gas outside of the PAR is calculated based on the following:

$$m_b c_{v,b} \frac{dT_{g,b}}{dt} = h_{wall} S_{wall} (T_{g,b} - T_{wall}) + \dot{m_{out}} c_{v,a} T_{g,a} - \dot{m_{in}} c_{v,b} T_{g,b} \quad (15)$$

where:

h_{wall} [W/(m^2 K)]: heat transfer coefficient between the confined space wall and the gas of the PAR;
T_{wall} [K]: temperature of the confined space wall which is assumed to be constant;
S_{wall} [m^2]: area.

3. GENERAL INSTRUCTIONS

3.1. INSTALLATION

The simulator software is available as an executable installer. The installer will install the application needed to enable user to run the PAR part-task simulator. A ".zip" file is provided, which can be uploaded to any folder or directly to the desired location. The user can create the shortcut of the launcher (.exe file) to the desired location.

3.2. START UP

Once the par-task simulator is installed, and shortcut created, follow these steps:

- Double click on the simulator's launcher, "PAR.exe', to start the simulator;
- Part-task simulator home page will appear as shown in FIG. 4;
- Click on the "Start" button;
- Part-task simulator is now ready, as shown in FIG. 5;
- The user can select the model to practice the exercises of which some are discussed in Section 4.

FIG. 4. PAR part-task simulator: home page.

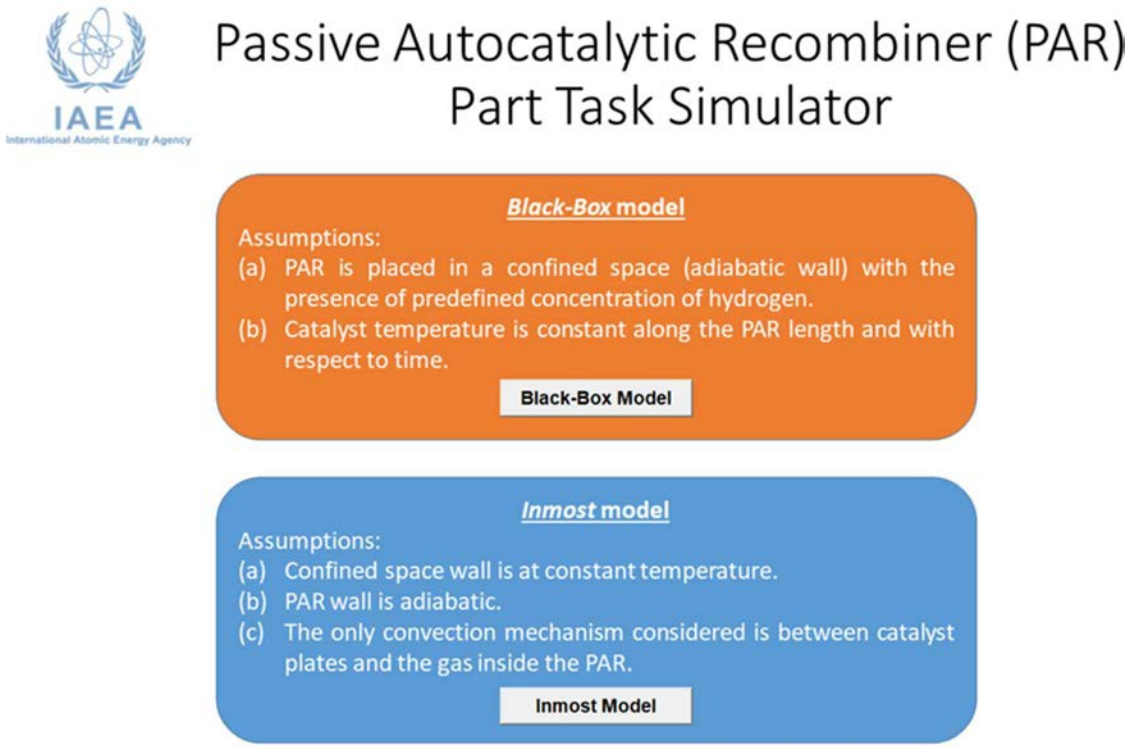

FIG. 5. PAR part-task simulator: selection of the simulation models.

3.3. SELECTION OF THE SIMULATION MODELS

The simulator has two models based on two different models of recombination:

- Black-box model;
- Inmost model.

To access one of these two models select the box as indicated in FIG. 5.

3.3.1. Black-box simulation model

The black-box model is used to study the PAR performance in a simplified manner. The PAR is located in a confined space (60 m^3) with the presence of pre-defined concentration of hydrogen.

The PAR is considered as a black-box; therefore, it is modelled based on a simplified hydrogen recombination rate equation, which only depends on hydrogen concentration and catalyst temperature. Such scenario creates a simplified hydrogen depletion transient and corresponding increase of temperature and pressure in the confined space. FIG. 6 shows the user interface of the black-box model. It displays a detailed and labelled schematics on the top and control buttons at the bottom.

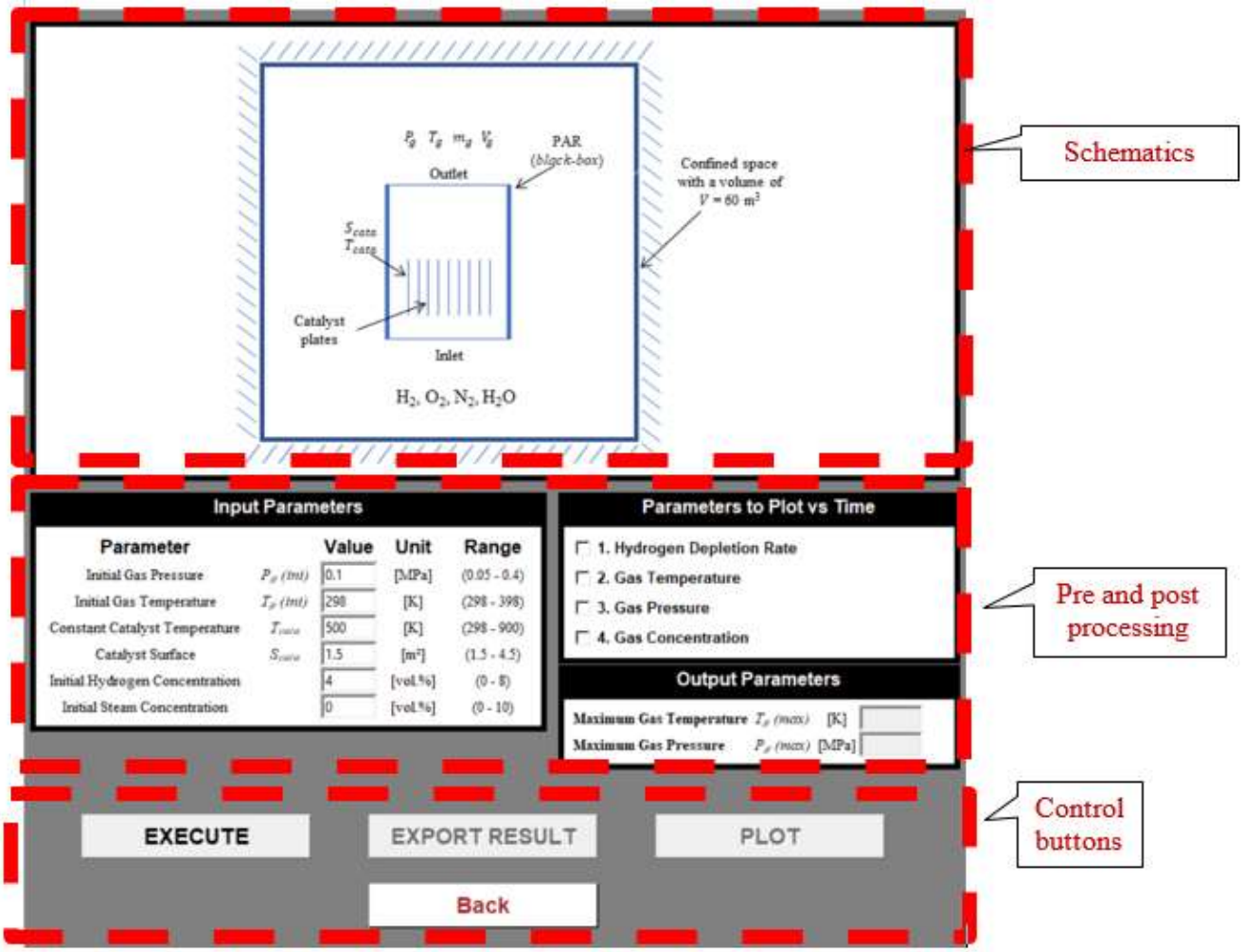

FIG. 6. PAR part-task simulator: black-box simulation model initiation.

Following are the three sections related to pre and post processing of the corresponding simulations:

- Input parameters;
- Parameters to plot variables as a function of time;
- Output parameters.

The input parameters to select are:

- Initial gas pressure;
- Initial gas temperature;
- Constant catalyst temperature;
- Catalyst surface;
- Initial hydrogen concentration;
- Initial steam concentration.

The first two parameters define the initial condition of the gas in the confined space. The following two parameters set the condition of the catalyst, which remain constant throughout recombination process, while the last two parameters set the initial amount of hydrogen and steam in the gas mixture. User can modify the preset values of these parameters. After setting input parameters the simulation is initiated by pressing “EXECUTE” button. Once the simulation is complete, the “EXPORT RESULT” and “PLOT” buttons appear available, and the part-task simulator presents the maximum values of the gas temperature and pressure in the “Output Parameter” section as shown in FIG. 7.

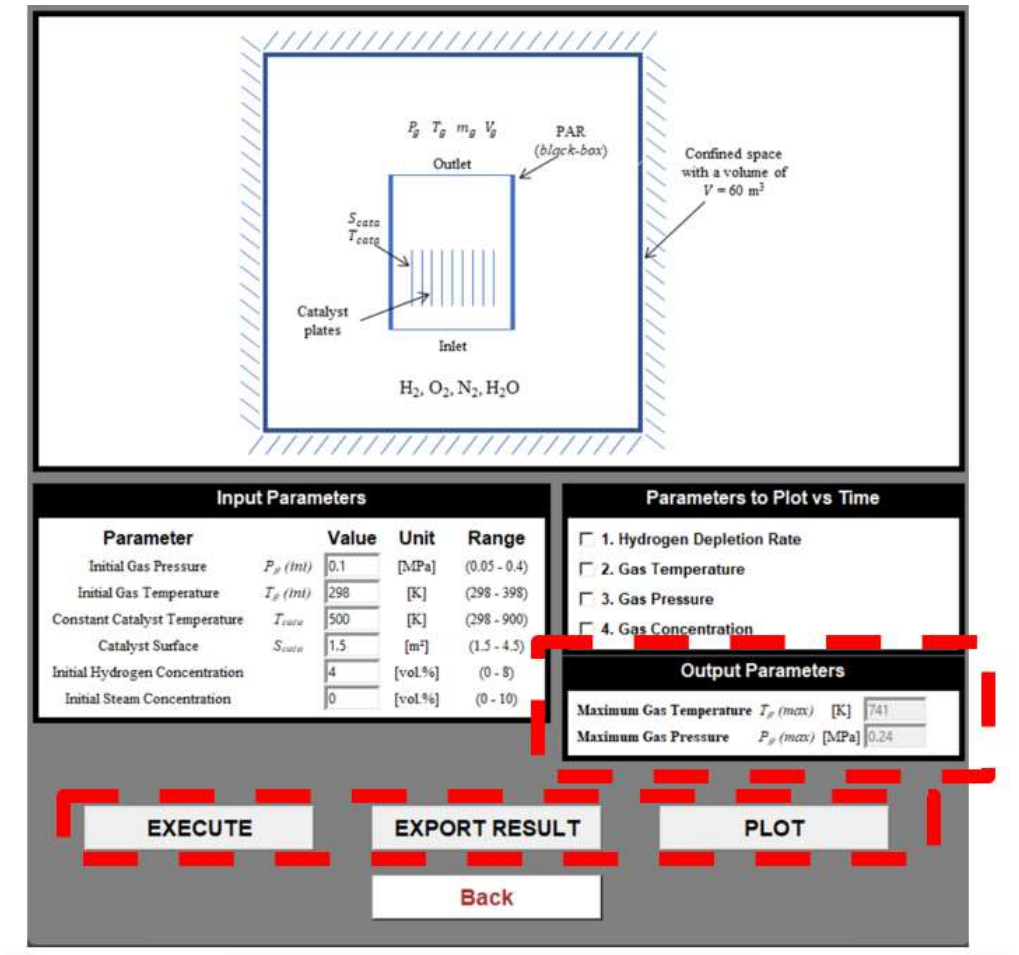

FIG. 7. PAR part-task simulator: black-box simulation model output values.

Parameters typical in showing the PAR behaviour and that can be selected to plot as a function of time are the hydrogen depletion rate, gas temperature, gas pressure, and gas concentration (hydrogen, oxygen, and steam concentration). By clicking on button “PLOT” the user can select more than one parameter to be displayed in a graph; example of hydrogen depletion rate change with time is shown in FIG. 8. There are few buttons at the bottom of the plot which allows a user to configure the plot, including zoom in, and also provides the option to save the graph.

The “EXPORT RESULT” button allows to export results of all the output parameters as a function of time in an Excel sheet which can be used for further postprocessing.

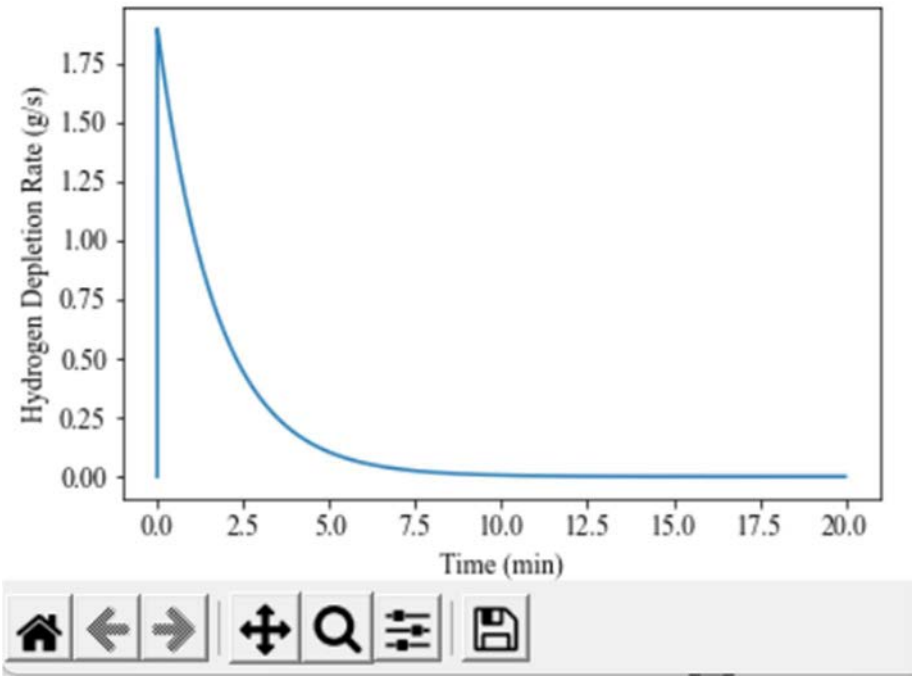

FIG. 8. PAR part-task simulator: hydrogen depletion rate as a function of time obtained using the black-box simulation model.

3.3.2. Inmost simulation model

The inmost simulation model provides to study PAR with more detailed operation as compared to the black-box mode. It assumes a confined space with a constant hydrogen injection from in-vessel and ex-vessel sources and differentiate between inside and outside PAR volumes. It also considers the effects of varying temperature of the catalyst.

FIG. 9 shows the interface map of the inmost mode. On the top, the schematics of the inmost PAR model is displayed with a list of fixed parameters with their numerical values. Fixed parameters include those related to PAR's geometry and the confined space conditions. There are pre and post processing sections in the middle and control buttons along with solution status bar displayed at the bottom. Following are the two sections in the middle related to pre and post processing of the simulation: input parameters and parameters to plot variables as a function of time.

In "Input parameters" section, the input variables with their symbols, typical values, units, and ranges are provided. Following is the list of considered input parameters:

- Initial gas pressure;
- Initial gas and catalyst temperature;
- Gas velocity inside of the PAR;
- Heat transfer coefficient (catalyst);
- Hydrogen injection rate;
- PAR start-up hydrogen concentration.

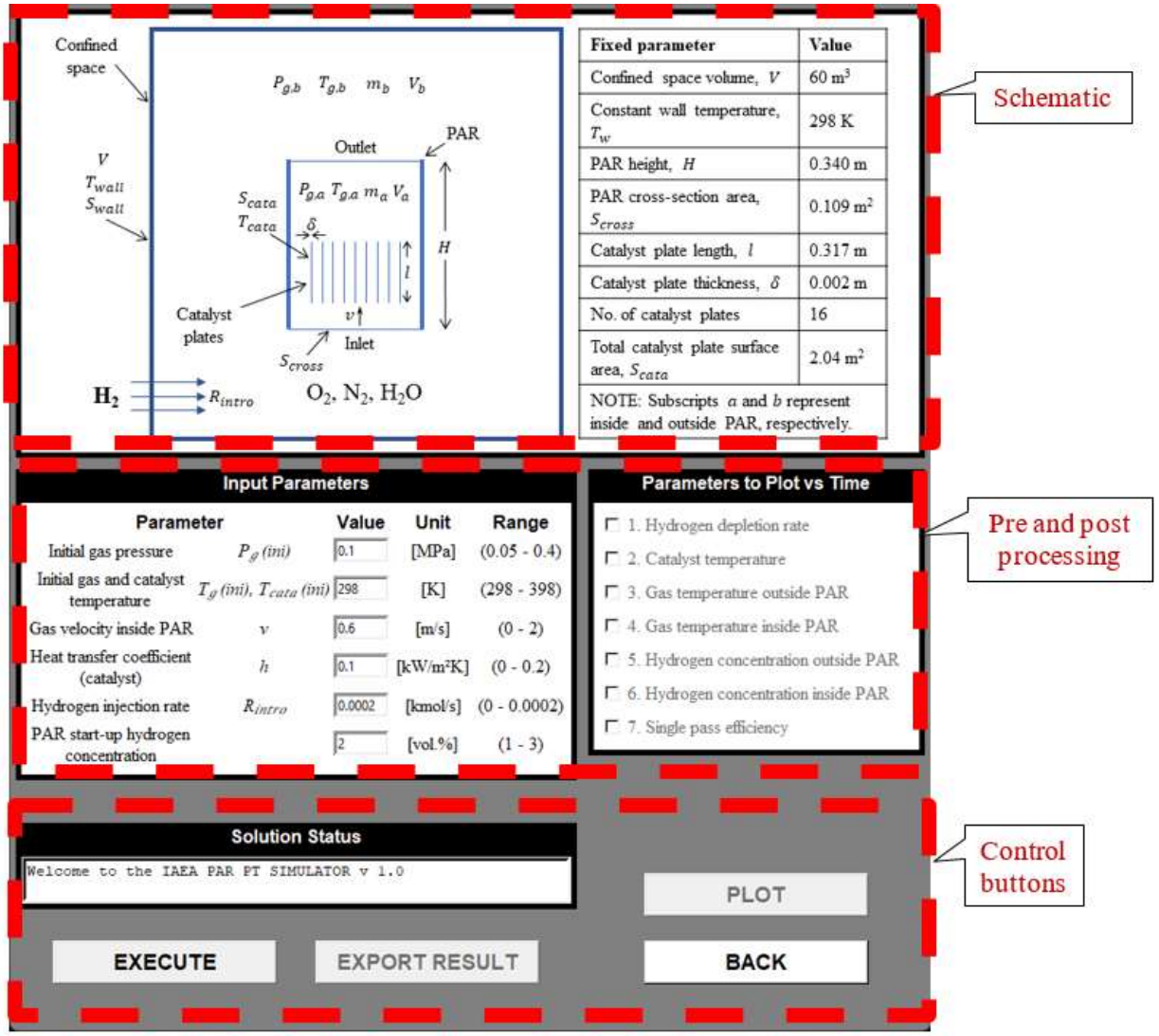

FIG. 9. PAR part-task simulator: inmost simulation model initiation.

These parameters include initial conditions of the PAR and its heat transfer capability. A constant "Hydrogen injection rate" into the confined space incorporates hydrogen generation. The input "PAR start-up hydrogen concentration" sets a threshold concentration of a hydrogen where PAR starts to work. User can modify typical preset values of these parameters. Clicking on the "EXECUTE" button starts the simulation and it takes a few seconds for simulation to complete. Once the simulation is complete the "Solution status" bar shows "Simulation is complete" and "EXPORT RESULT" and "PLOT" buttons become available as shown FIG. 10.

Following is the list of parameters which can be plotted against time in "Parameters to Plot vs Time" section:

— Hydrogen depletion rate;
— Catalyst temperature;
— Gas temperature outside of the PAR;
— Gas temperature inside the PAR;

— Hydrogen concentration outside of the PAR;
— Hydrogen concentration inside the PAR;
— Single pass efficiency.

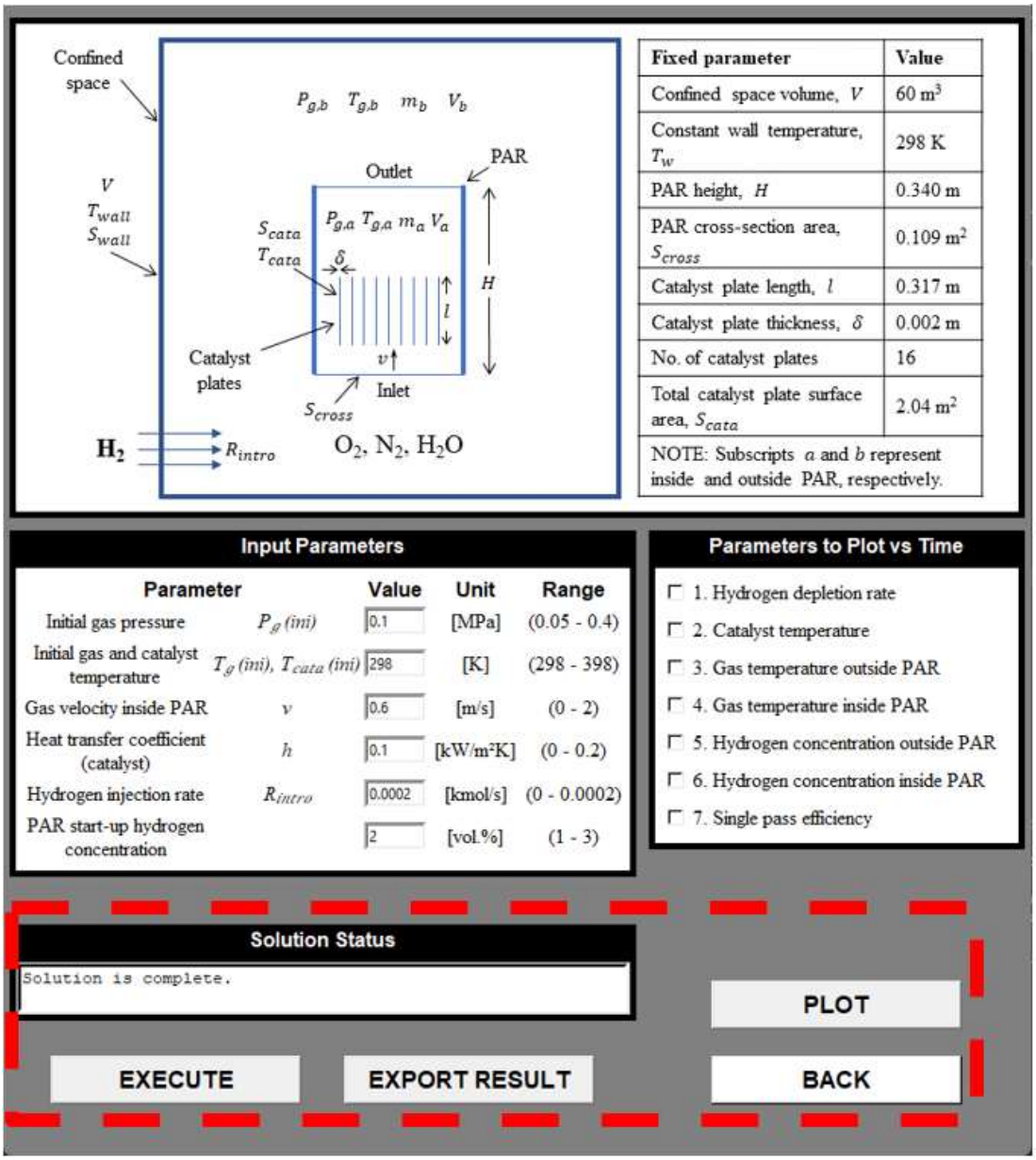

FIG. 10. PAR part-task simulator: inmost simulation model output values.

The hydrogen depletion rate and the catalyst temperature show the catalyst performance. Since the inmost model differentiates between the inside and outside conditions of the PAR, it provides separate plots for temperature and hydrogen concentration. It also provides a single pass efficiency plot with time as it varies with hydrogen concentration inside and outside of the PAR. User can select multiple parameters to plot by clicking the relevant checkboxes and clicking the “PLOT” corresponding plots are generated; example of hydrogen depletion rate as a function of time is shown in FIG. 11. The “EXPORT RESULT” button allows to export results

of all the output parameters as a function of time in an Excel sheet which can be used for further postprocessing.

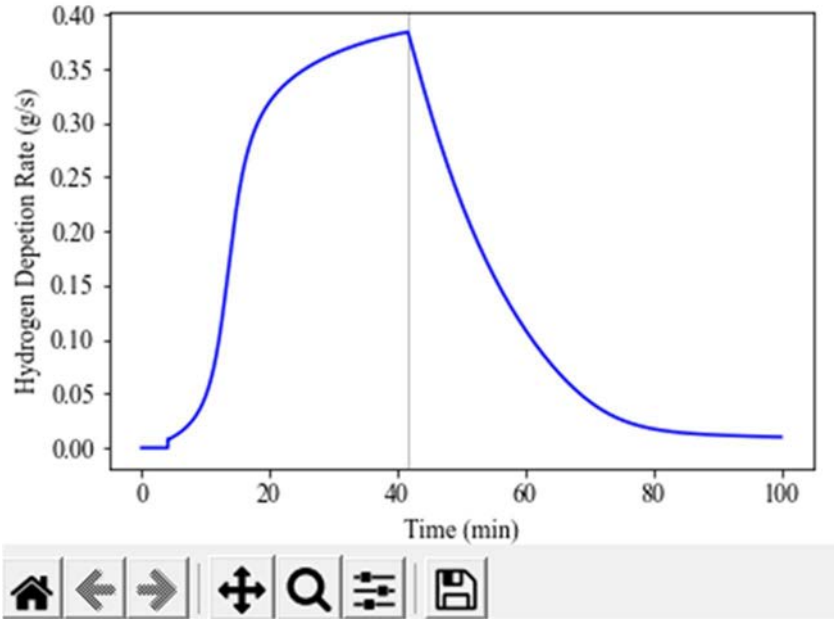

FIG. 11. PAR part-task simulator: hydrogen depletion rate as a function of time obtained using the inmost simulation model.

4. EXAMPLES

All the figures in this publication are screen shots of the simulator display and plots generated by the PAR part-task simulator. The following are examples workable for self-learning and to be used in education and training workshops.

The following section provides descriptions of the six specific examples:

- Adiabatic isochoric combustion (black-box model);
- Variation of catalyst surface area (black-box model);
- Variation of initial steam concentration (black-box model);
- Effect of low inlet gas velocity (inmost model);
- Effect of high inlet gas velocity (inmost model);
- Effect of heat transfer coefficient (inmost model).

4.1. ADIABATIC ISOCHORIC COMBUSTION (BLACK-BOX MODEL)

In this example, the PAR part-task simulator black-box model is used to study the trends of hydrogen depletion rate, gas temperature, gas pressure, and gas concentration. The example assumes constant volume and the air around the PAR is not replacing that increases the gas temperature and pressure around the PAR due to exothermic reaction between hydrogen and oxygen. The initial temperature and pressure around the PAR are assumed to be the same as that of the containment pressure and temperature under normal conditions (i.e., atmospheric

pressure and temperature). The assumed constant catalyst temperature in real scenario changes along the PAR surface. The constant initial hydrogen concentration is also assumed.

4.1.1. Simulation steps

In Step 1, click on the 'Simulator' button as shown in FIG. 4, and described in the Section 3.1. In Step 2, select the 'Black-Box Model' to initiate the 'Black-Box' mode as shown in FIG. 12.

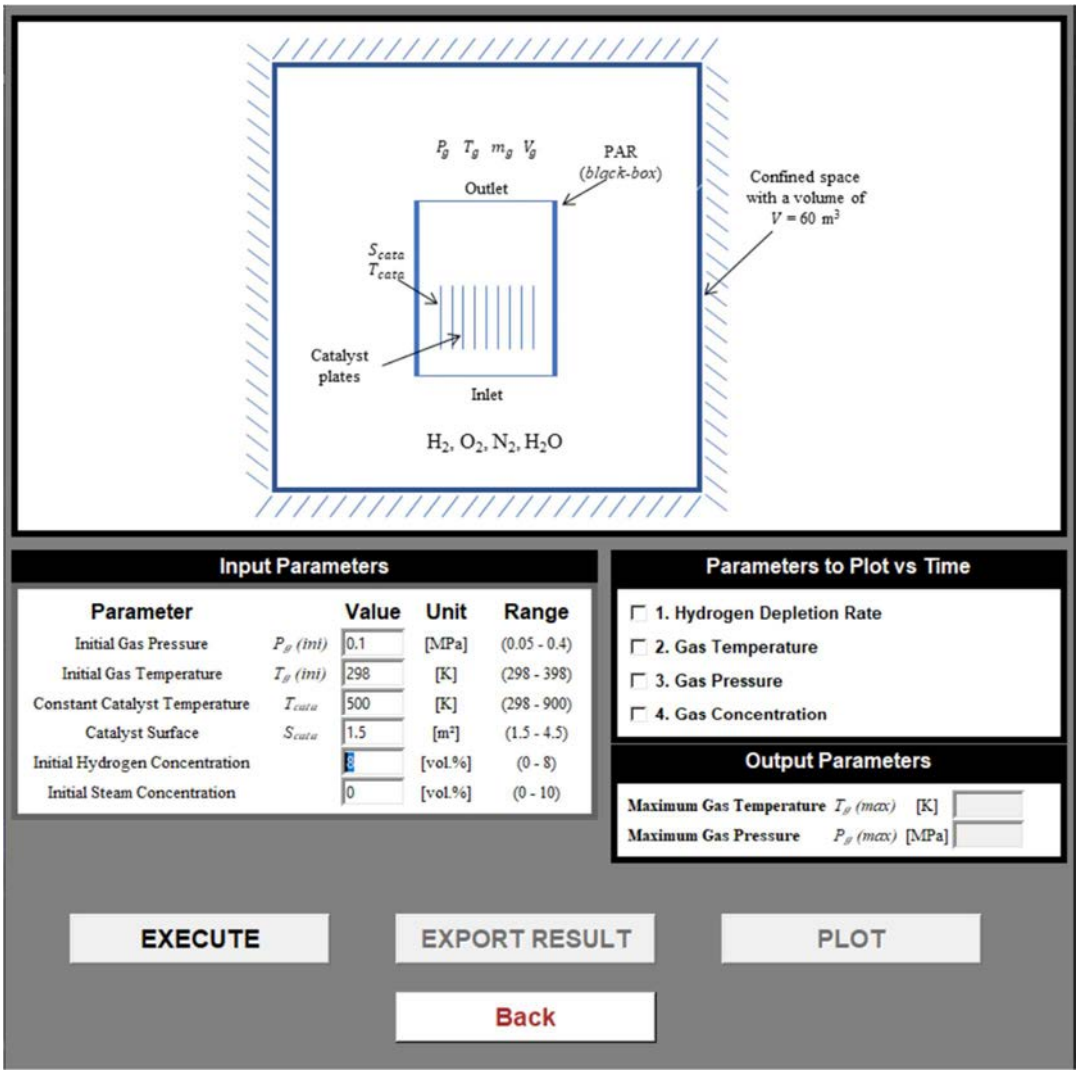

FIG. 12. PAR part-task simulator: input parameters in the example of adiabatic isochoric combustion (black-box model).

In Step 3, specify the input parameters as example shown in TABLE 1. All of the input parameters are set by default except for the initial hydrogen concentration. In Step 4, click the 'EXECUTE' button as shown in FIG. 12, and wait until the calculations are completed. The 'EXPORT RESULT' button and 'PLOT' button will become available after calculations are completed as shown in FIG. 13. In Step 5, check the 'Hydrogen Depletion Rate' box under 'Parameters to Plot vs Time', and then click 'PLOT' button to view the results, as shown in FIG. 16. Then repeat the Step 5 for 'Gas Temperature' (FIG. 14), 'Gas Pressure' (FIG. 15), and 'Gas Concentration' (FIG. 17).

TABLE 1. INPUT PARAMETERS FOR THE EXAMPLE OF ADIABATIC ISOCHORIC COMBUSTION (BLACK-BOX MODEL)

Input Parameters	Value	Range
Initial gas pressure [MPa]	0.1	0.05–0.4
Initial gas temperature [K]	298	298–398
Constant catalyst temperature [K]	500	298–900
Catalyst surface area [m^2]	1.5	1.5–4.5
Initial hydrogen concentration [vol/ %]	8	0–8
Initial steam concentration [vol. %]	0	0–10

4.1.2. Analysis of the output parameters

FIG. 13 shows maximum gas temperature (example value of 1,145 K) and pressure (example value of 0.37 MPa) as provided under the 'Output Parameters' heading.

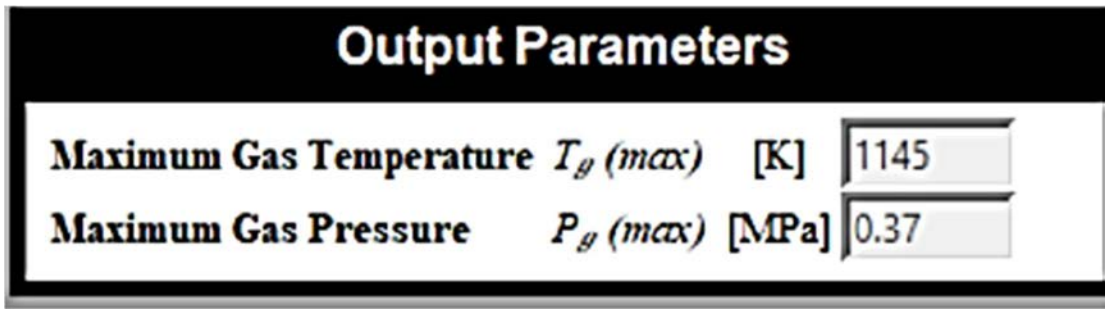

FIG. 13. PAR part-task simulator: output parameters in the example of adiabatic isochoric combustion (black-box model).

FIG. 14 shows the increase in gas temperature as a function of time. The gas temperature increases exponentially from 298 K to 1,145 K in just 10 minutes and then remains constant at that temperature because of adiabatic wall conditions of the confined space.

The gas pressure trend is shown in FIG. 15; it can be observed that it increases exponentially from 0.1 MPa to 0.37 MPa in 10 minutes due to adiabatic isochoric combustion. After 10 minutes the gas pressure remains steady at 0.37 MPa. The time dependent behaviour of gas pressure and gas temperature is directly linked to hydrogen depletion rate whereas the maximum temperature and pressure in the confined space are linked to initial hydrogen and steam concentration.

FIG. 16 shows variation of hydrogen depletion rate inside the imaginary confined volume as a function of time. The hydrogen depletion rate exponentially decreases from 3.6 g/s at the start of simulation to 0 g/s in 10 minutes. After 10 minutes the hydrogen depletion rate remains at the zero value. The hydrogen depletion rate depends on hydrogen remaining in the bulk flow inside the PAR, the catalyst temperature, and the catalyst surface available for the combustion reaction.

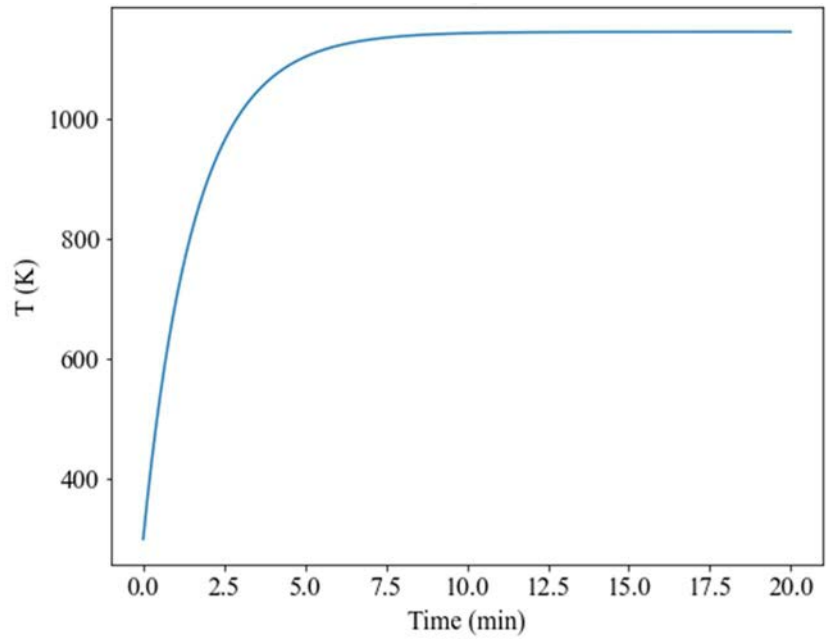

FIG. 14. PAR part-task simulator: gas temperature as a function of time in the example of adiabatic isochoric combustion (black-box model).

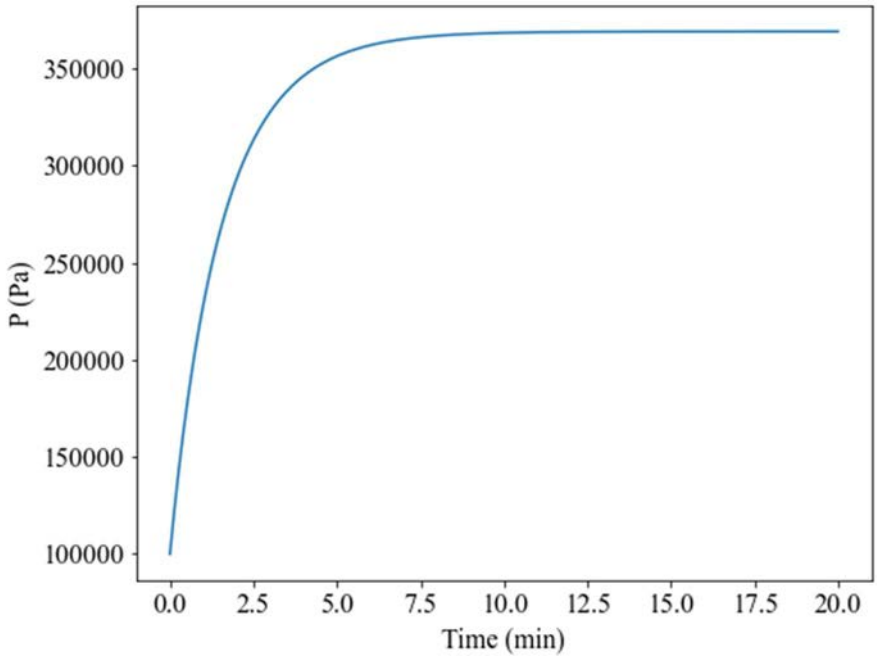

FIG. 15. PAR part-task simulator: gas pressure as a function of time in the example of adiabatic isochoric combustion (black-box model).

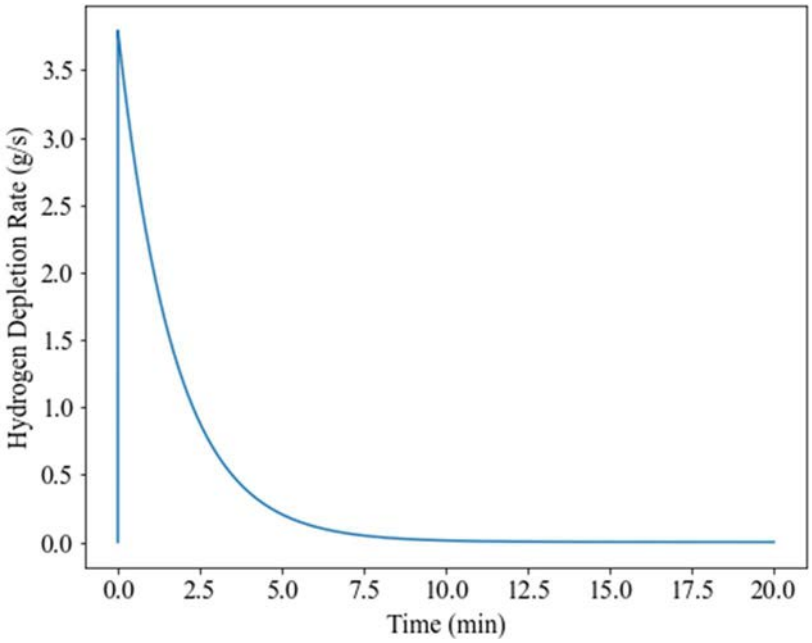

FIG. 16. PAR part-task simulator: hydrogen depletion rate as a function of time in the example of adiabatic isochoric combustion (black-box model).

FIG. 17 shows the concentration of hydrogen, oxygen, and steam as a function of time in the confined space. In the first 10 minutes, the hydrogen concentration in the confined space decreases from 8 vol.% to 0 vol.%. The steam concentration increases from 0 vol.% to 7.5 vol.%, and the oxygen concentration decreases from 19 vol.% to 16 vol.%. Therefore, the PAR converted all initially available hydrogen to steam in just 10 minutes.

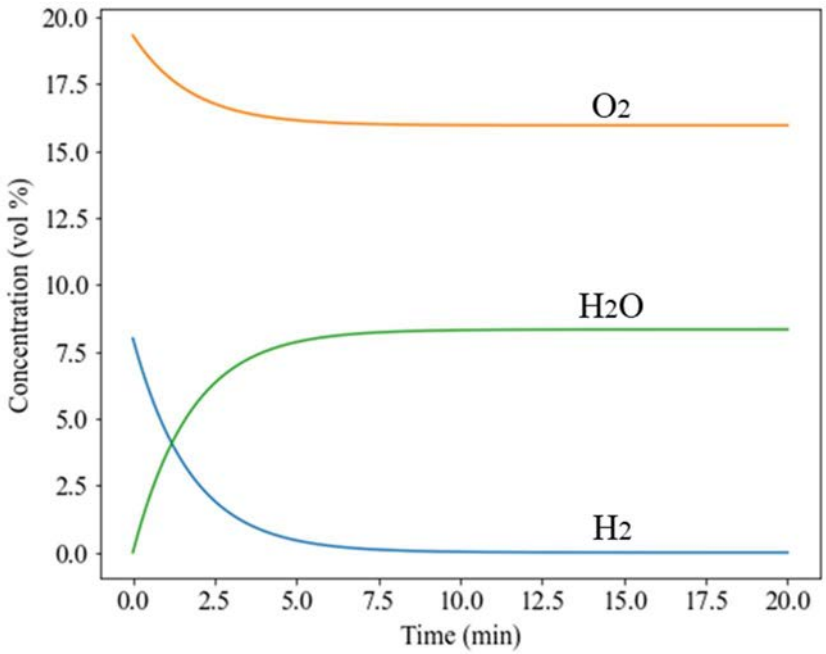

FIG. 17. PAR part-task simulator: gas/steam concentration as a function of time in the example of adiabatic isochoric combustion (black-box model).

4.2. VARIATION OF CATALYST SURFACE AREA (BLACK-BOX MODEL)

In this example, the effect of the PAR catalyst surface area on hydrogen depletion rate, gas temperature, gas pressure, and gas concentration are discussed. Increasing the catalyst surface area increases the hydrogen depletion rate, which in turns changes the PAR parameters.

4.2.1. Simulation steps

The simulation follows the same steps as described in Section 4.1.1 with changing 'Catalyst Surface' to 4.0 m^2 as shown in FIG. 18. Then the steps are repeated by changing the 'Catalyst Surface' area from 2.0 m^2 to 3.5 m^2 with an increment of 0.5 m^2 to observe during which time the initial hydrogen depletion rate and hydrogen concentration reach zero.

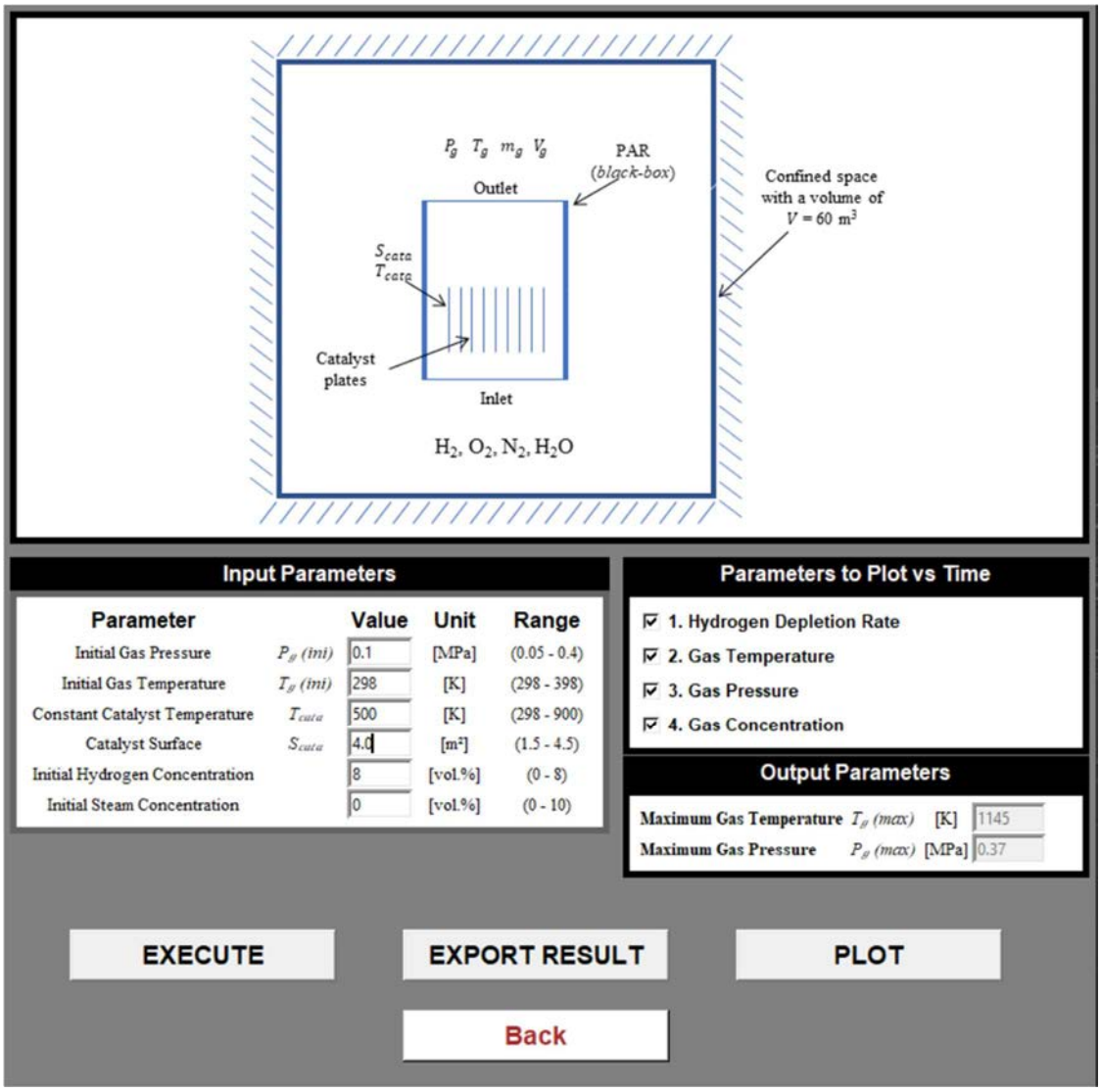

FIG. 18. PAR part-task simulator: input parameters for the example of varied catalyst surface area (black-box model).

4.2.2. Analysis of the output parameters

FIG. 18 shows the maximum gas temperature and maximum gas pressure as a function of time for the catalyst surface of 4.0 m^2 (found under 'Output Parameters'). The maximum values of gas temperature and pressure are same as for the example shown in Section 4.1, because the initial hydrogen and steam concentration are equal in both cases. FIG. 19 shows the variation of gas temperature with time; the maximum gas temperature is reached in less than 5 minutes. FIG. 20 shows the variation of pressure with time; it follows similar trend as gas temperature.

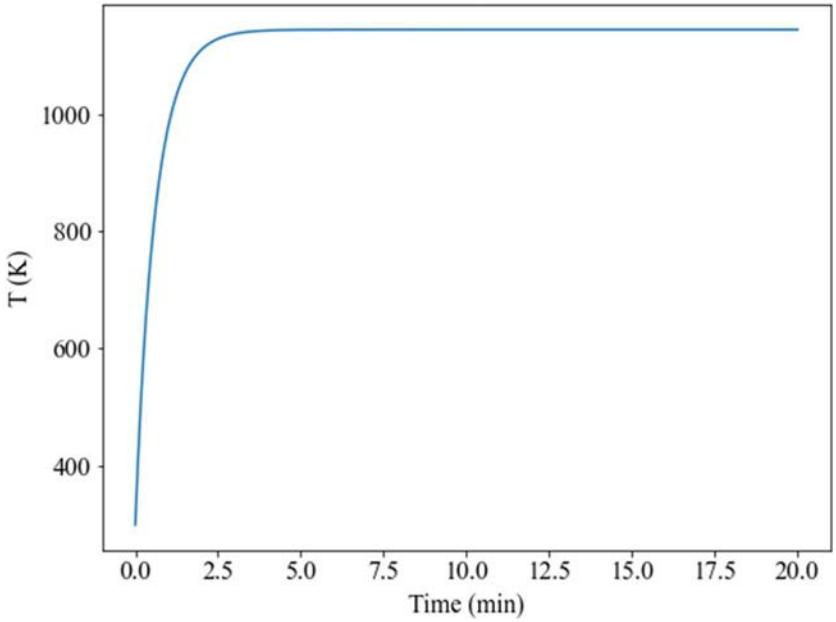

FIG. 19. PAR part-task simulator: gas temperature as a function of time in the example of varied catalyst surface area (black-box model).

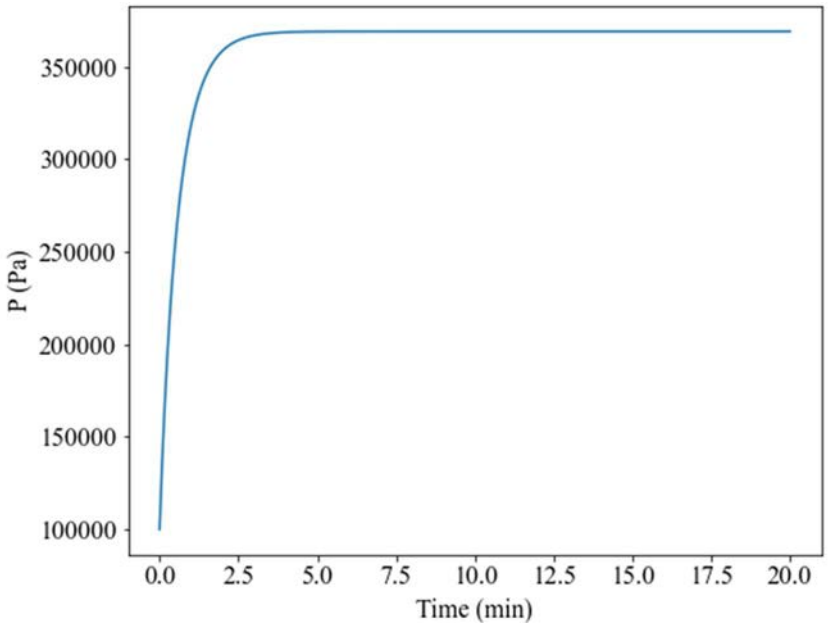

FIG. 20. PAR part-task simulator: gas pressure as a function of time in the example of varied catalyst surface area (black-box model).

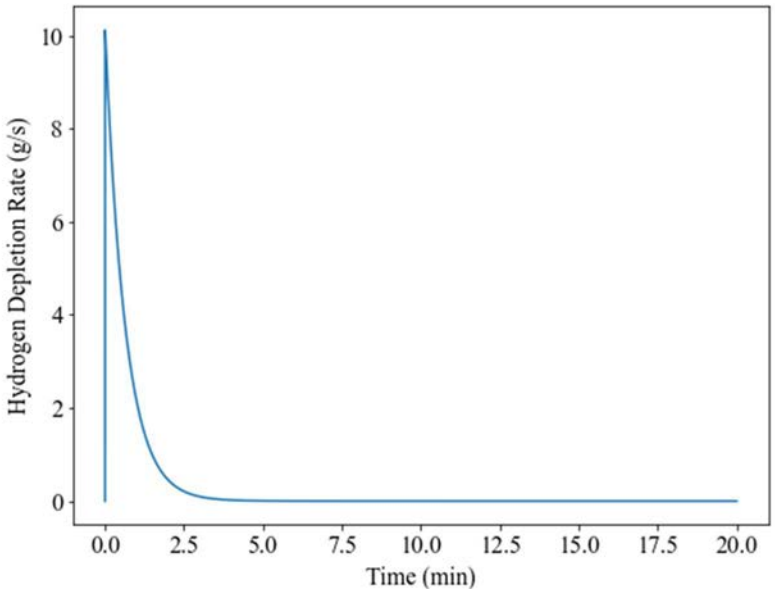

FIG. 21. PAR part-task simulator: hydrogen depletion rate as a function of time in the example of varied catalyst surface area (black-box model).

FIG. 21 shows time variation of hydrogen depletion rate at catalyst surface of 4.0 m^2. It can be observed that the initial hydrogen depletion rate decreases from 10 g/s which is higher than the one obtained for the example described in Section 4.1, because of larger surface area. The hydrogen depletion rate decreases from 10 g/s to 0 g/s in 3 minutes, showing that all of hydrogen is converted to steam. The change of catalyst surface area affects the time during which the hydrogen is converted into steam as seen in FIG. 22 with total amount of hydrogen converted to steam remaining the same. It also shows that the final steam and oxygen concentrations are as well the same as in the example described in Section 4.1.

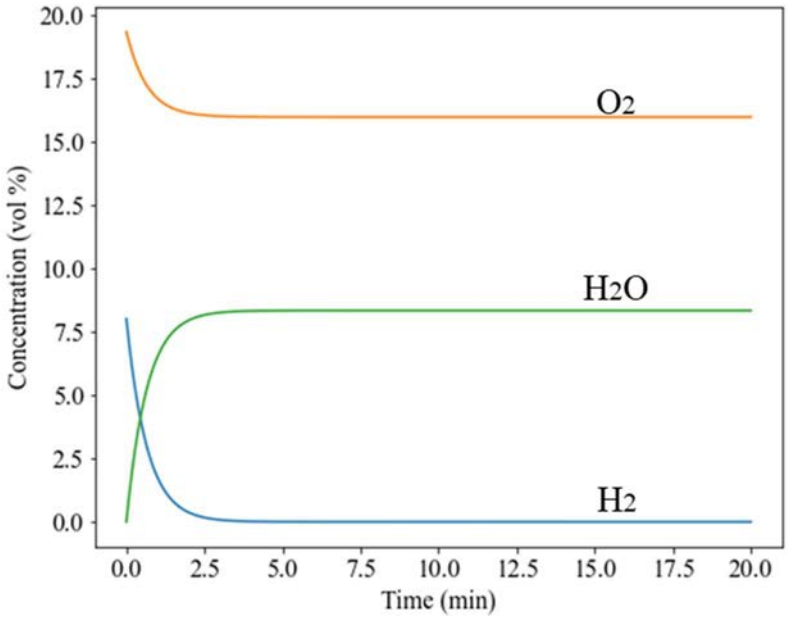

FIG. 22. PAR part-task simulator: gas/steam concentration as a function of time in the example of varied catalyst surface area (black-box model).

TABLE 2 shows initial hydrogen depletion rate and total time needed for conversion of hydrogen to steam for different catalyst surface areas. The initial hydrogen depletion rate increases linearly with increase of catalyst surface temperature; however, total time for the complete conversion of hydrogen decreases exponentially with increase of catalyst surface temperature. It can be seen that the PAR size affects the time for complete hydrogen conversion up to a certain limit. After that the size does not have any notable effect on the conversion time.

TABLE 2. INITIAL HYDROGEN DEPLETION RATE AND HYDROGEN CONVERSION TIME FOR DIFFERENT CATALYST SURFACE AREAS (BLACK-BOX MODEL)

Catalyst surface area (m^2)	Initial hydrogen depletion rate (g/s)	Time for complete conversion of hydrogen (min)
2.0	5.0	7.5
2.5	6.3	5.0
3.0	7.6	3.8
3.5	8.9	3.6

4.3. VARIATION OF INITIAL STEAM CONCENTRATION (BLACK-BOX MODEL)

In this example, the black-box model is used to study the effect of initial steam concentration on hydrogen depletion rate, gas temperature, gas pressure, and gas concentration.

4.3.1. Simulation steps

This simulation follows the same steps as described in Section 4.2.1 with changing 'Initial Steam Concentration' to 5 vol.%, as shown in TABLE 3. Then the initial steam concentration is changed from 1 vol.% to 7 vol.% with increment of 1 vol.% to observe the change in maximum gas temperature and final steam concentration.

TABLE 3. INPUT PARAMETERS FOR THE EXAMPLE OF VARIATION OF INITIAL STEAM CONCENTRATION (BLACK-BOX MODEL)

Input Parameters	Value	Range
Initial gas pressure [MPa]	0.1	0.05–0.4
Initial gas temperature [K]	298	298–398
Constant catalyst temperature [K]	500	298–900
Catalyst surface area [m^2]	4.0	1.5–4.5
Initial hydrogen concentration [vol.%]	8	0–8
Initial steam concentration [vol.%]	5	0–10

4.3.2. Analysis of the output parameters

FIG. 23 shows the maximum gas temperature of 1,134 K and pressure of 0.37 MPa. The maximum gas pressure is same as obtained in the example provided in Section 4.2. The maximum gas temperature is lower than the one obtained in the example described in Section 4.2. The decrease in maximum gas temperature is due to initial steam concentration values.

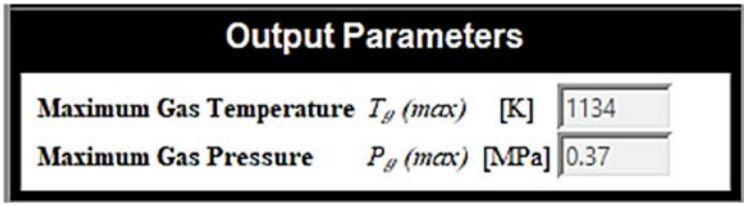

FIG. 23. PAR part-task simulator: output parameters for the example of variation of initial steam concentration (black-box model).

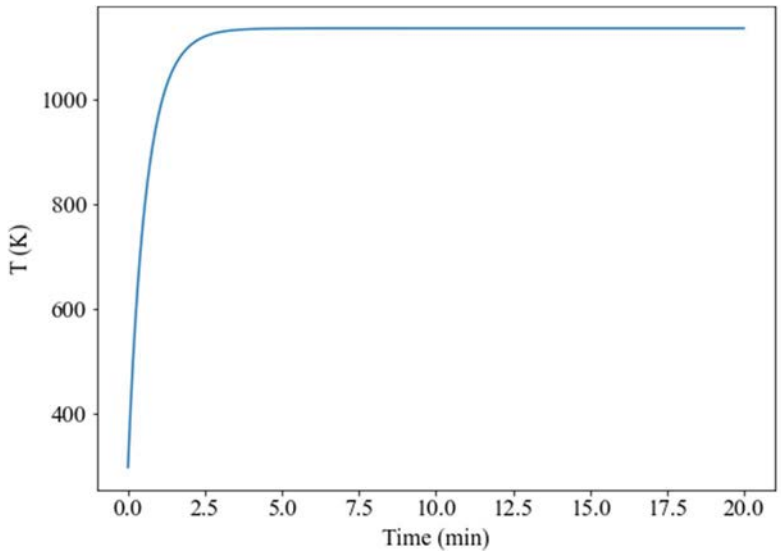

FIG. 24. PAR part-task simulator: gas temperature as a function of time in the example of variation of initial steam concentration (black-box model).

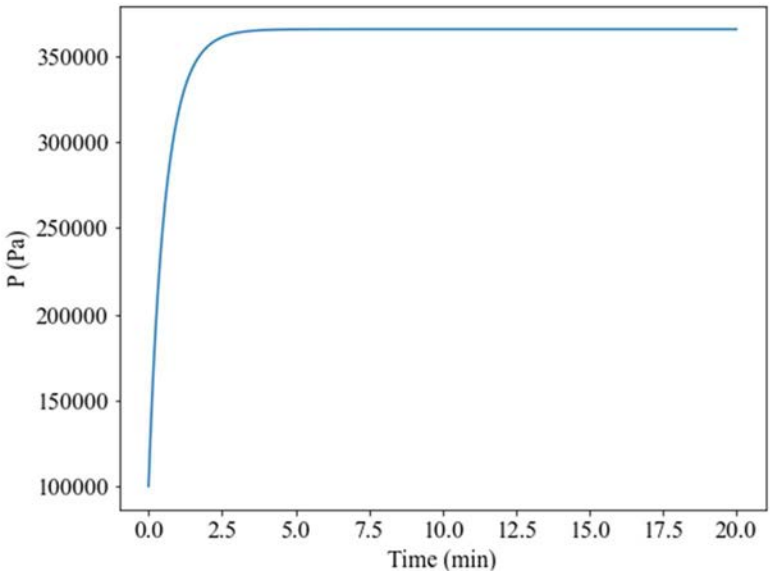

FIG. 25. PAR part-task simulator: gas pressure as a function of time in the example of variation of initial steam concentration (black-box model).

FIG. 24 shows gas temperature change with time. It can be seen that it increases exponentially from 298 K to 1,134 K in 3 minutes, after which it remains constant due to the adiabatic wall conditions of the confined space. The gas pressure follows similar trend (FIG. 25). The initial

steam concentration does not affect the trend of the gas pressure. The decrease in maximum gas pressure is very small. This effect is more pronounced at higher steam concentrations. The hydrogen depletion rate is not affected by initial steam concentration as seen in FIG. 26. The trend is exactly like in the example described in Section 4.2.

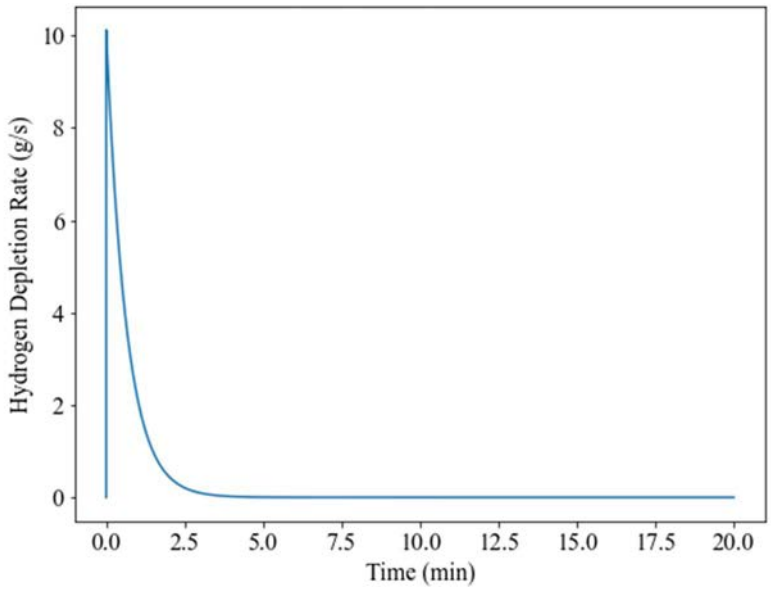

FIG. 26. PAR part-task simulator: hydrogen depletion rate as a function of time in the example of variation of initial steam concentration (black-box model)).

FIG. 27 shows the variation of hydrogen, oxygen, and steam concentration with time. The oxygen concentration decreases from 18 vol.% to 14 vol.% and the hydrogen concentration decreases from 8 vol.% to 0 vol.% in 3 minutes, whereas steam concentration increases from 5 vol.% to 12.5 vol.%, because of oxygen and hydrogen recombination.

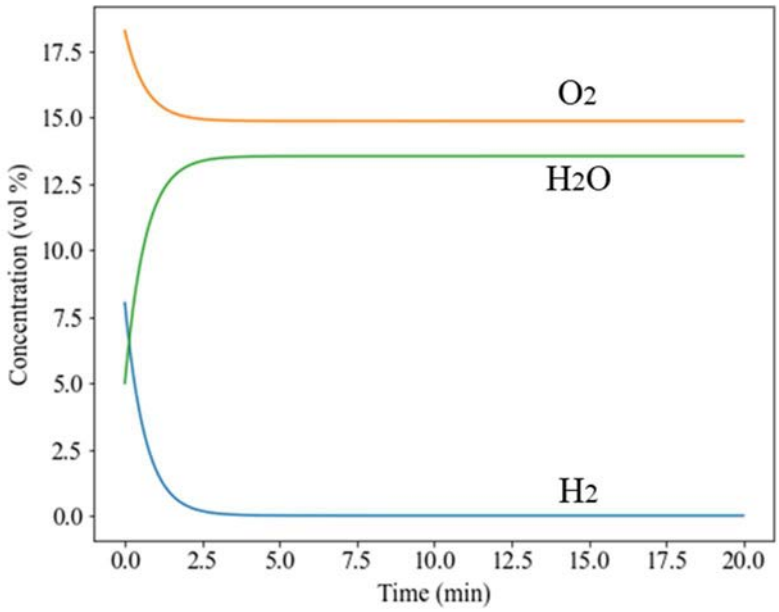

FIG. 27. PAR part-task simulator: gas/steam concentration as a function of time in the example of variation of initial steam concentration (black-box model)

TABLE 4 lists maximum gas temperatures and maximum steam concentrations inside the PAR. The maximum gas temperature decreases linearly from 1,143 K to 1,124 K as the initial steam concentration increases from 1 vol.% to 10 vol.%. Similarly, the maximum steam concentration after complete conversion of hydrogen to steam also increases from 9.4 vol.% to 17.7 vol.%.

TABLE 4. EFFECT OF INITIAL STEAM CONCENTRATION ON PAR PARAMETERS (BLACK-BOX MODEL)

Initial steam concentration (vol.%)	Maximum gas temperature (K)	Maximum steam concentration (vol.%)
1	1,143	9.4
2	1,140	10.4
3	1,138	11.4
4	1,136	12.5
5	1,134	13.5
6	1,132	14.6
7	1,130	15.6

4.4. EFFECT OF LOW INLET GAS VELOCITY (INMOST MODEL)

In this example, the inmost mode is used to study the change of hydrogen depletion rate, catalyst temperature, gas temperature outside of the PAR, gas temperature inside the PAR, hydrogen concentration outside of the PAR, hydrogen concentration inside the PAR, and single pass efficiency as a function of time for low inlet gas velocity. The air around the PAR is continuously replacing, and the volume around the PAR is assumed to be fixed with constant wall temperature. The PAR parameters are shown in FIG. 28.

4.4.1. Simulation steps

In Step 1, select ‘Simulator’ button as shown in FIG. 4, and as described in Section 3.1. In Step 2, select the ‘Inmost Model’ as indicated in FIG. 28. In Step 3, specify the input parameters as shown in FIG. 28.

All of the input parameters are set by default except for the gas pressure. In Step 4, click the ‘EXECUTE’ button, and wait until the calculations are completed. In Step 5, select ‘Hydrogen Depletion Rate’ box under ‘Parameters to Plot vs Time’ and then click the ‘PLOT’ button to view the results, as shown in FIG. 29.

To study the parameters trends, then repeat Step 5 for ‘Catalyst Temperature’ (FIG. 30), ‘Gas Temperature Outside PAR’ (FIG. 31), ‘Gas Temperature Inside PAR’ (FIG. 32), ‘Hydrogen Concentration Outside PAR’ (FIG. 33), ‘Hydrogen Concentration Inside PAR’ (FIG. 34), and ‘Single Pass Efficiency’ (FIG. 35). The following section outlines the trends of these parameters as a function of time.

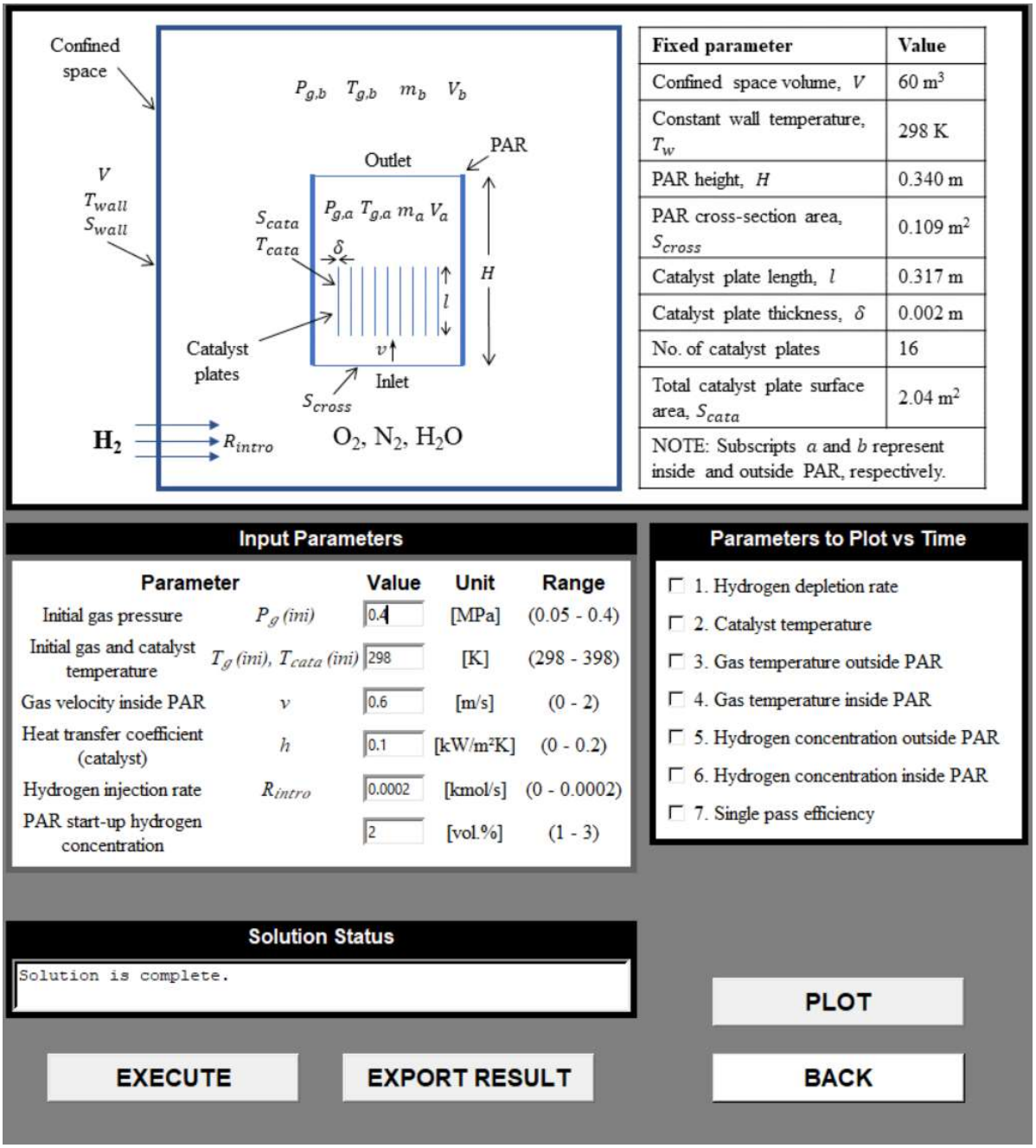

FIG. 28. PAR part-task simulator: input parameters for the example of low inlet gas velocity (inmost model).

4.4.2. Analysis of the output parameters

FIG. 29 shows the variation of hydrogen depletion rate with time. At the start of simulation, the hydrogen depletion rate is zero and then increases as PAR starts its operation, after 18th minute of simulation. It continues to increase exponentially until it reaches a steady state value, of ~0.4 g/s. The steady state value represents the equilibrium between hydrogen injection and hydrogen recombination in the PAR. After about 40 minutes, the second phase of calculation starts, in which the hydrogen injection to PAR is stopped. At this point the hydrogen depletion rate as expected decreases.

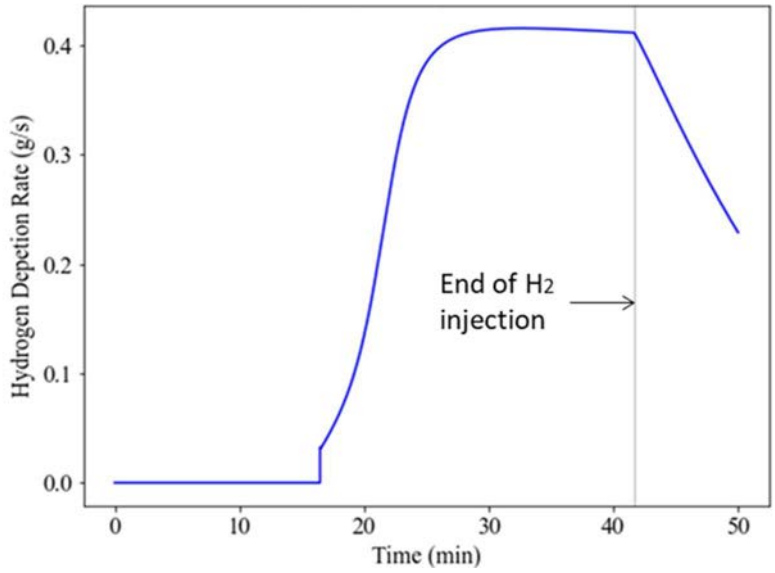

FIG. 29. PAR part-task simulator: hydrogen depletion rate as a function of time in the example of low inlet gas velocity (inmost model).

FIG. 30 shows the variation of catalyst temperature with time. It can be seen that the trend is similar to hydrogen depletion rate variation with time. When the PAR starts its operation, hydrogen combines with oxygen in exothermic reaction, that produces the heat, which increases the catalyst temperature. The increase in catalyst temperature affects the hydrogen depletion rate positively. The maximum catalyst temperature at steady state is approaching 800 K; after which it starts to decrease when the hydrogen injection to PAR is stopped.

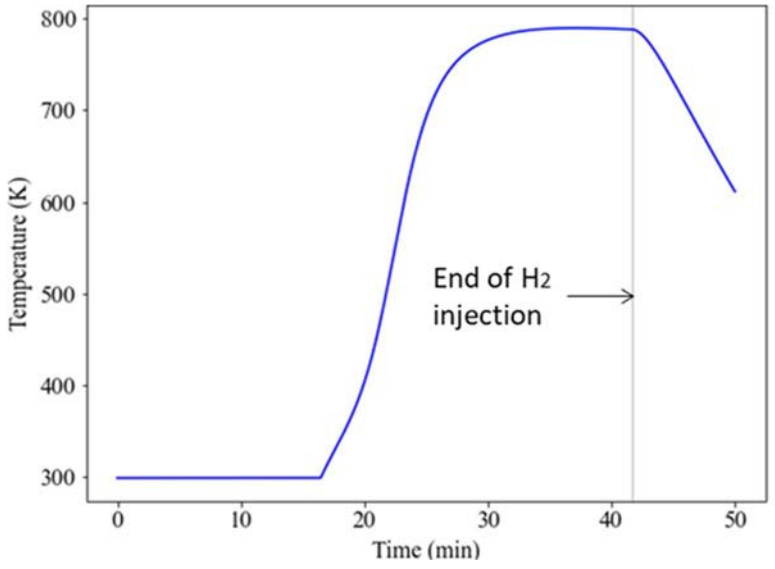

FIG. 30. PAR part-task simulator: catalyst temperature as a function of time in the example of low inlet gas velocity (inmost model).

FIG. 31 shows the variation of gas temperature outside of the PAR. The minimum gas temperature outside the PAR is the atmospheric temperature of 298 K before the PAR starts its operation. This temperature increases then exponentially to 355 K. The maximum gas temperature outside the PAR is lower than maximum catalyst temperature, which shows that

the heat is being transferred from the catalyst plates. After hydrogen injection is stopped, it decreases following similar trend as the catalyst temperature.

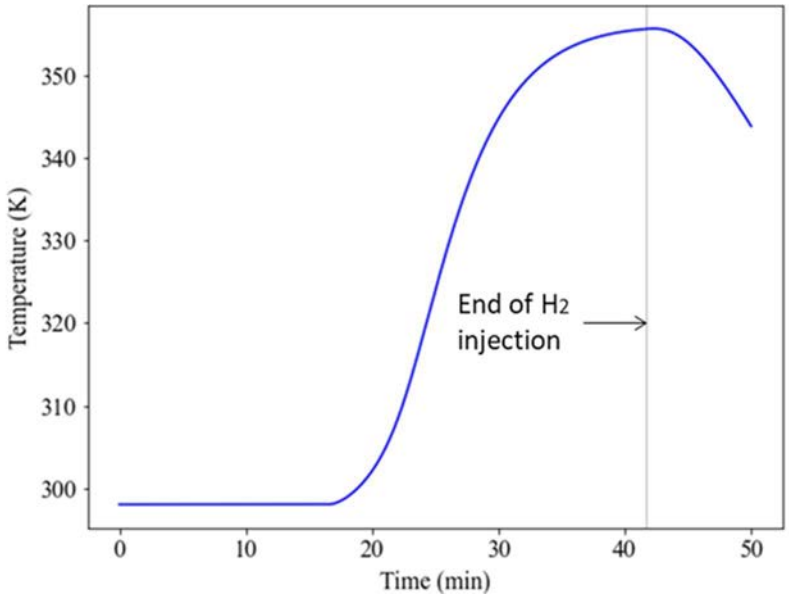

FIG. 31. PAR part-task simulator: gas temperature outside the PAR as a function of time in the example of low inlet gas velocity (inmost model).

FIG. 32 shows the time variation of gas temperature inside the PAR, which is similar to the catalyst temperature change inside the PAR. The maximum gas temperature inside the PAR of 550 K lies in between the maximum catalyst temperature of 800 K and the maximum gas temperature outside the PAR of 355 K. It can be seen from FIG. 30, FIG. 31, and FIG. 32 show that, after hydrogen injection is stopped, the catalyst temperature suddenly decreases but the gas temperature inside and outside the PAR decreases after short time because of the time needed for the heat to move from catalyst surface to the gas outside the PAR.

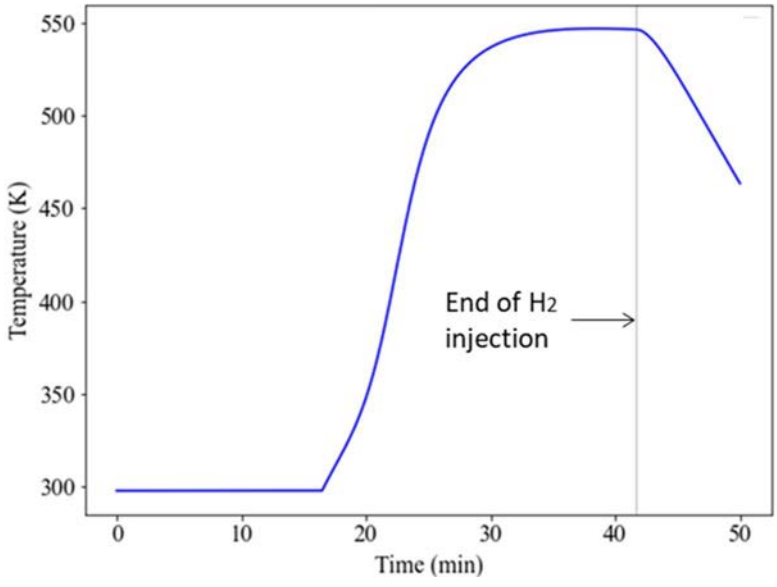

FIG. 32. PAR part-task simulator: gas temperature inside the PAR as a function of time in the example of low inlet gas velocity (inmost model).

FIG. 33 shows the change of hydrogen concentration outside the PAR with time. It increases from 0 to a maximum value of 2.5 vol.%; then it decreases slowly as the PAR starts its operation. This decrease is due to an imbalance between the hydrogen injection and hydrogen recombination. When the hydrogen injection is stopped, the hydrogen concentration outside the PAR rapidly decreases.

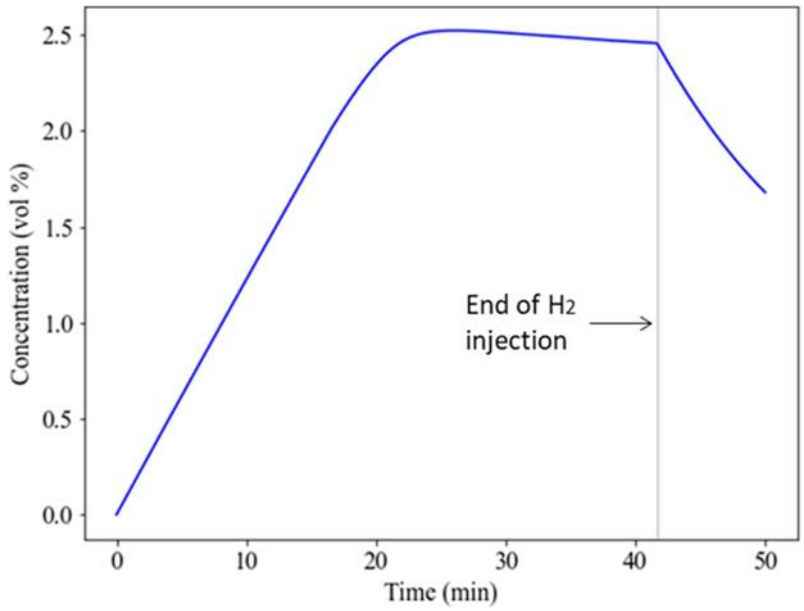

FIG. 33. PAR part-task simulator: hydrogen concentration outside the PAR as a function of time in the example of low inlet gas velocity (inmost model).

FIG. 34 shows the time variation of hydrogen concentration inside the PAR. It increases from the beginning of the simulation until it reaches the PAR start-up hydrogen concentration specified as the input value of 2 vol.%. After this, the hydrogen recombination process starts that decreases hydrogen concentration inside the PAR from 2 vol.% to ~0.5 vol.% (steady state). At the end of hydrogen injection, there exists a large difference between the hydrogen concentration inside and outside of the PAR. Thus, the hydrogen concentration inside the PAR tends to reach the hydrogen concentration outside the PAR and vice versa. The PAR is continuously converting hydrogen to steam even after hydrogen injection is stopped. Therefore, after some time the hydrogen concentrations inside and outside of the PAR decrease in consistency with each other thereby decreasing the overall concentration in the confined space.

FIG. 35 shows the time dependence of a PAR's single pass efficiency. After hydrogen concentration reaches the PAR start-up concentration, there is a rapid increase in single pass efficiency, which then slowly converges to about 75% at the steady state when there is an equilibrium between hydrogen recombination inside the PAR and hydrogen injection rate. When hydrogen injection is stopped at about 42nd minute, the single pass efficiency of the PAR decreases because of a decrease in catalyst temperature and the reduction in hydrogen concentration outside the PAR.

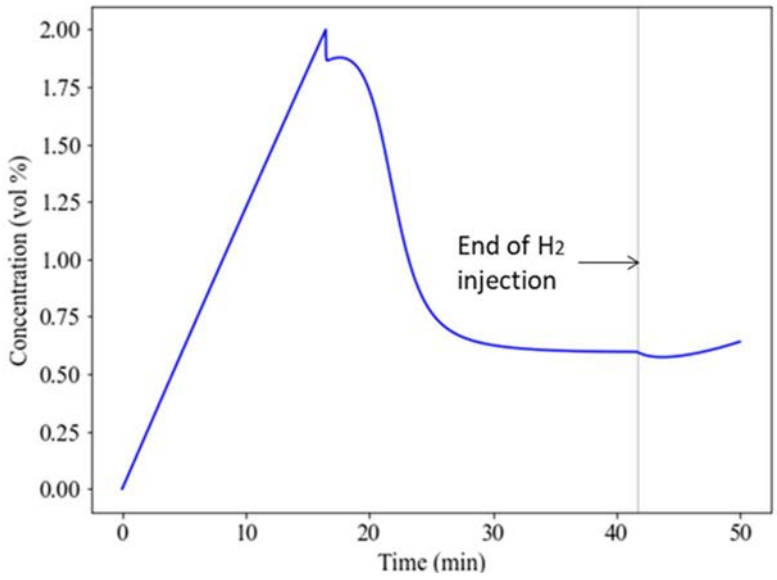

FIG. 34. PAR part-task simulator: hydrogen concentration inside the PAR as a function of time in the example of low inlet gas velocity (inmost model).

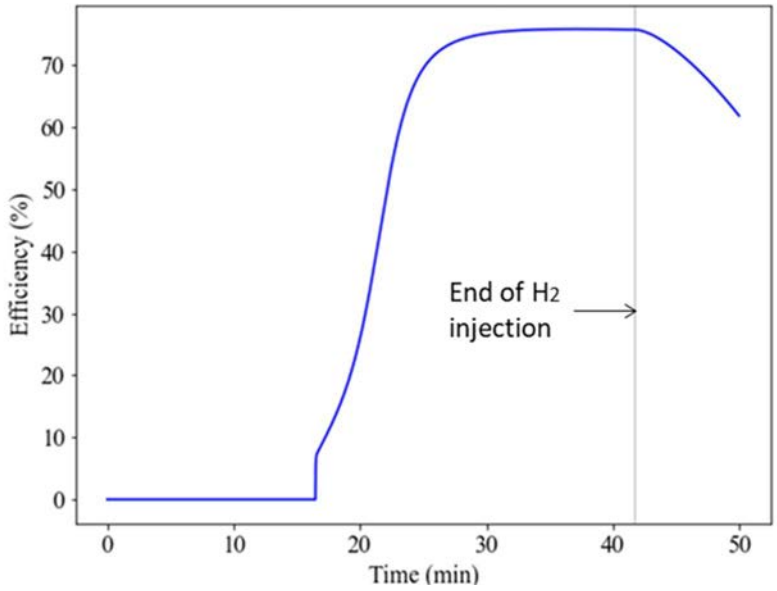

FIG. 35. PAR part-task simulator: single pass efficiency of the PAR as a function of time in the example of low inlet gas velocity (inmost model).

4.5. EFFECT OF HIGH INLET GAS VELOCITY (INMOST MODEL)

In this example, the inmost model is used to study hydrogen depletion rate, catalyst temperature, gas temperature outside PAR, gas temperature inside PAR, hydrogen concentration outside PAR, hydrogen concentration inside PAR, and single pass efficiency at high inlet gas velocity. Increasing gas velocity inside the PAR increases the maximum catalyst temperature.

4.5.1. Simulation steps

This simulation follows the same steps as described in Section 4.4.1 with changing 'Gas Velocity Inside PAR' to 2 m/s as shown in FIG. 28.

4.5.2. Analysis of the output parameters

FIG. 36 shows the variation of hydrogen depletion rate with time. Increasing the gas inlet velocity does not affect the PAR start-up time as long as the hydrogen injection rate remains the same. Thus, the start-up time is the same as in the example described in Section 4.4 (i.e., 18 minutes). Hydrogen depletion rate increases rapidly after the PAR start-up from 0 g/s to 1.0 g/s and then it decreases rapidly. The steady state value is not reached. Initially, the increase in hydrogen depletion rate is the result of high inlet gas velocity and PAR inside hydrogen concentration, as shown in FIG. 41.

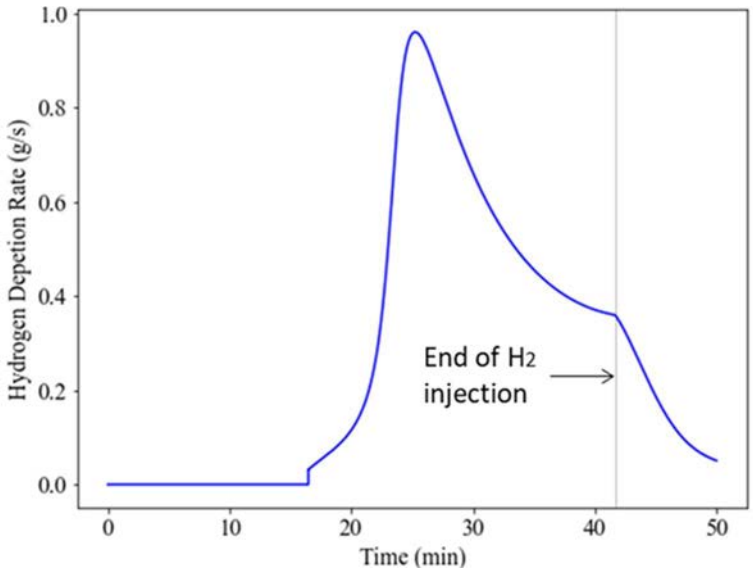

FIG. 36. PAR part-task simulator: hydrogen depletion rate as a function of time in the example of high inlet gas velocity (inmost model).

The recombination of hydrogen increases the catalyst temperature, which in turns increases hydrogen depletion rate. The increased inlet velocity enhances the heat transfer. Therefore, after some time the catalyst temperature decreases. The combined effect of decreased catalyst temperature and the reduction in hydrogen concentration decreases the hydrogen depletion rate. After hydrogen injection is stopped, the hydrogen depletion rate continues to decrease. FIG. 37 shows the variation of catalyst temperature with time; it follows the similar trend as hydrogen depletion rate. The maximum catalyst temperature is obtained when hydrogen depletion rate is maximum, which is near 1,000 K. The catalyst temperature affects the performance of the PAR such as hydrogen depletion rate, which in turns affects the catalyst temperature. The higher the hydrogen depletion rate, the higher is the catalyst temperature keeping all other parameters constant because of large amount of hydrogen conversion in a short period of time.

FIG. 38 and FIG. 39 show the variation of gas temperatures outside and inside the PAR with time, respectively. The trend of both, the gas temperature outside and inside the PAR, is similar to the catalyst temperature change with time. The maximum gas temperature inside the PAR is 500 K and the one outside the PAR is 390 K. The slight time shift when compared to the catalyst temperature change with time, is due to the time needed for the heat to move from the catalyst

plate to outside of the PAR. This heat transfer is due both the circulation inside and outside the PAR and the conduction through the PAR wall.

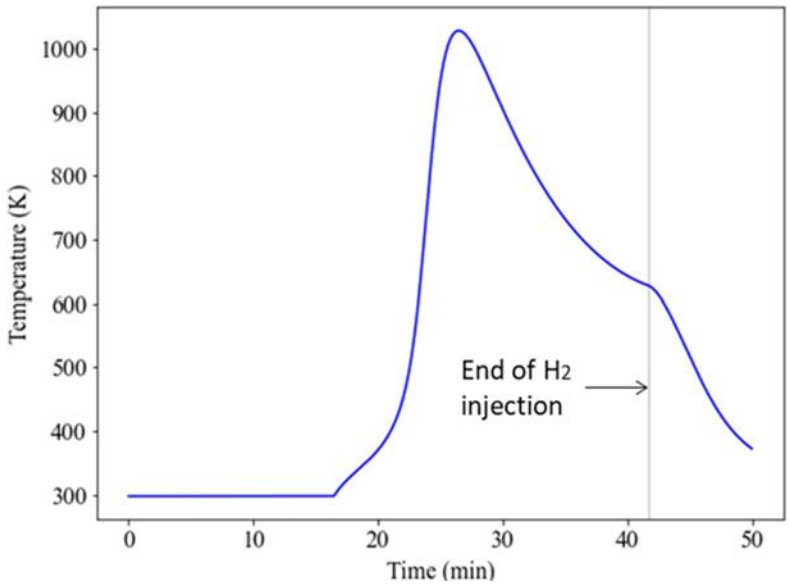

FIG. 37. PAR part-task simulator: catalyst temperature rate as a function of time in the example of high inlet gas velocity (inmost model).

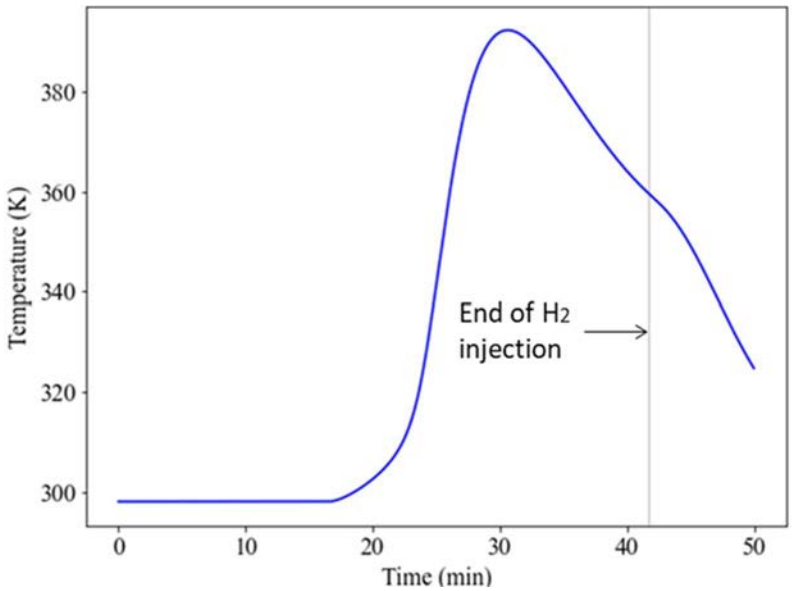

FIG. 38. PAR part-task simulator: gas temperature outside the PAR rate as a function of time in the example of high inlet gas velocity (inmost model).

FIG. 40 and FIG. 41 show the variation of hydrogen concentration outside and inside the PAR, respectively. The hydrogen concentration inside the PAR is not affected by the increase of gas velocity as the hydrogen injection rate is the same as described in Section 4.4 before the PAR start-up concentration is achieved. After the PAR start-up, the hydrogen concentration inside the PAR continuous to increase unlike in the example described in Section 4.4, because the high gas inlet velocity replaces the air inside the PAR more rapidly. The rapid increase in hydrogen concentration inside the PAR increases the hydrogen depletion rate (FIG. 36) and the catalyst temperature (FIG. 37) which in turns reverses the trend of hydrogen concentration

inside the PAR that starts to decrease. The decrease in hydrogen concentration also affects the hydrogen depletion rate and decreases it thereby decreasing the catalyst temperature as well. This trend continues until the PAR enters the second phase of operation when the hydrogen injection to the confined space is stopped. The concentration difference between the inlet and outlet of the PAR causes a slight increase in hydrogen concentration inside the PAR. The recombination of hydrogen is still going on inside the PAR, which eventually decreases the hydrogen concentration inside and outside the PAR.

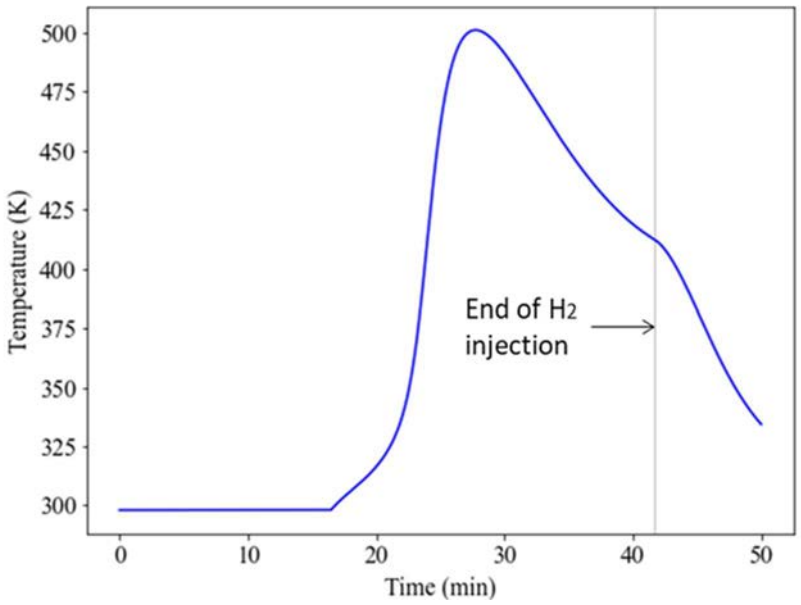

FIG. 39. PAR part-task simulator: gas temperature inside the PAR rate as a function of time in the example of high inlet gas velocity (inmost model).

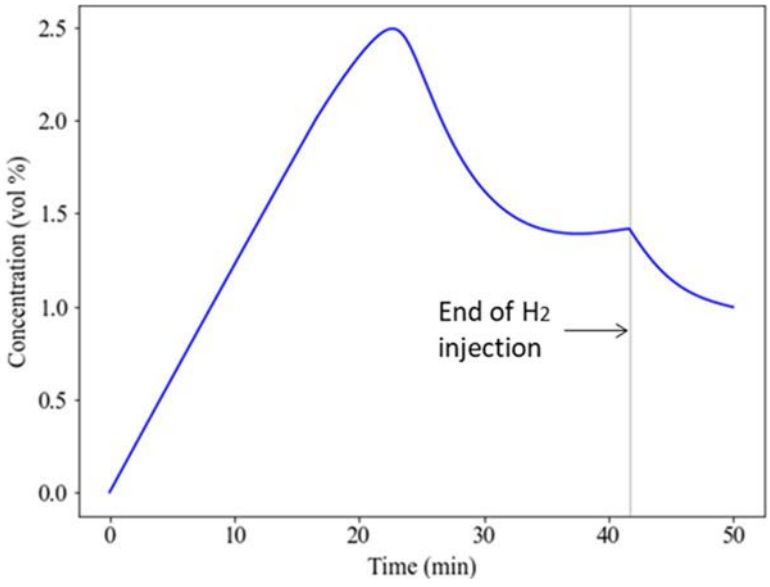

FIG. 40. PAR part-task simulator: hydrogen concentration outside the PAR rate as a function of time in the example of high inlet gas velocity (inmost model).

The hydrogen concentration outside the PAR decreases more slowly than the hydrogen concentration inside the PAR, because the hydrogen inside and outside the PAR is separated by the wall. The inside hydrogen is continuously in contact with catalyst plates and undergoes

recombination. During the second phase of PAR operation, the hydrogen concentration outside the PAR is continuously decreasing unlike the hydrogen concentration inside the PAR.

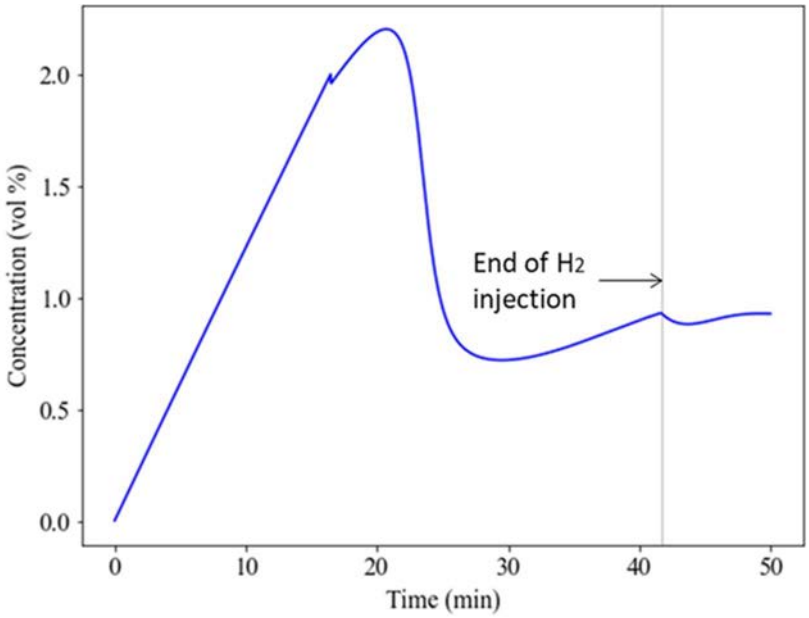

FIG. 41. PAR part-task simulator: hydrogen concentration inside the PAR rate as a function of time in the example of high inlet gas velocity (inmost model).

FIG. 42 shows the variation of single pass efficiency of PAR at high inlet gas velocity. The single pass gas efficiency decreases because at high velocity the contact time between the catalyst plates and the gas is decreased, which in turns reduces the single pass efficiency of the PAR. The maximum single pass efficiency occurs at the point of the highest hydrogen depletion rate of 60 %. During the second phase of PAR operation, the single pass efficiency decreases rapidly.

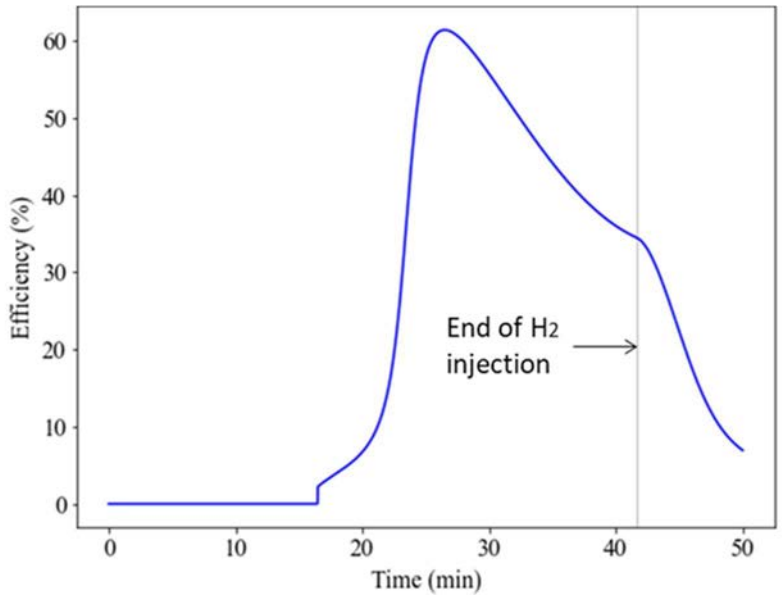

FIG. 42. PAR part-task simulator: single pass efficiency of the PAR rate as a function of time in the example of high inlet gas velocity (inmost model).

4.6. EFFECT OF HEAT TRANSFER COEFFICIENT (INMOST MODEL)

In this example, the effect of heat transfer coefficient is studied using the inmost mode. This example represents an extension of the previous example in which the heat transfer coefficient is changed while keeping all other parameters same. The increase in heat transfer coefficient decreases the catalyst temperature, which in turn decreases the hydrogen depletion rate, gas temperature outside and inside the PAR, and the single pass efficiency. However, the hydrogen concentration inside and outside the PAR is increased.

4.6.1. Simulation steps

This simulation follows the same steps as described Section 4.4.1 by changing the heat transfer coefficient from 0.1 $kWm^{-2}K^{-1}$ to 0.2 $kWm^{-2}K^{-1}$ with increment of 0.02 $kWm^{-2}K^{-1}$.

4.6.2. Analysis of the output parameters

FIG. 43 shows the variation of hydrogen depletion rate with time for the maximum heat transfer coefficient of 0.2 $kWm^{-2}K^{-1}$ and the maximum gas velocity of 2 m/s. It follows similar trend of the example discussed in Section 4.5.2, except that the peak value of the hydrogen depletion rate occurs after 30 minutes of PAR operation. There is an increase in hydrogen depletion rate as shown in TABLE 5. The increase in heat transfer coefficient does not affect the hydrogen depletion rate directly, but it influences the catalyst temperature (FIG. 44), which then affects the hydrogen depletion rate.

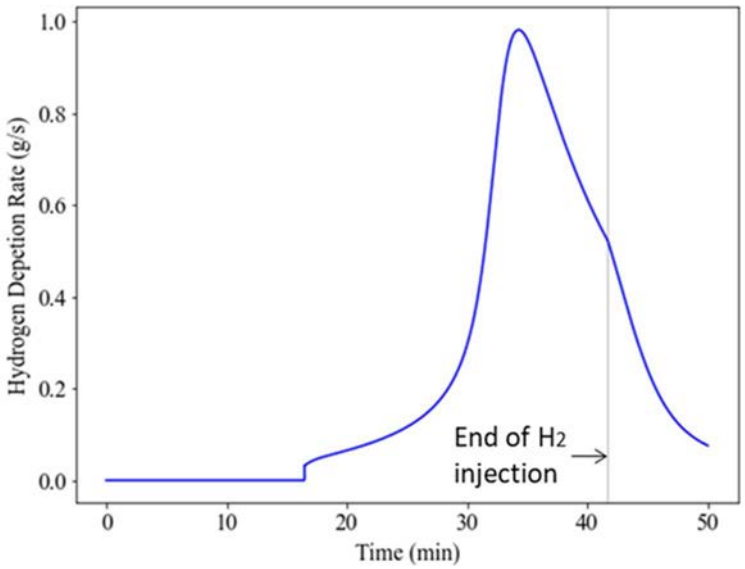

FIG. 43. PAR part-task simulator: hydrogen depletion rate as a function of time in the example of heat transfer coefficient effects (inmost model).

FIG. 44, FIG. 45 and FIG. 46 show the time variation of the catalyst temperature, gas temperature outside the PAR and the gas temperature inside the PAR, respectively.

The trends are similar to the ones obtained in the example described in Section 4.5.2. However, the maximum value of catalyst temperature in this case is smaller, because increase in heat

transfer coefficient. Since the gas temperatures inside and outside the PAR are greatly influenced by the catalyst temperature, they also decrease with catalyst temperature. The maximum gas temperature outside the PAR is 400 K whereas the maximum gas temperature inside the PAR is 750 K.

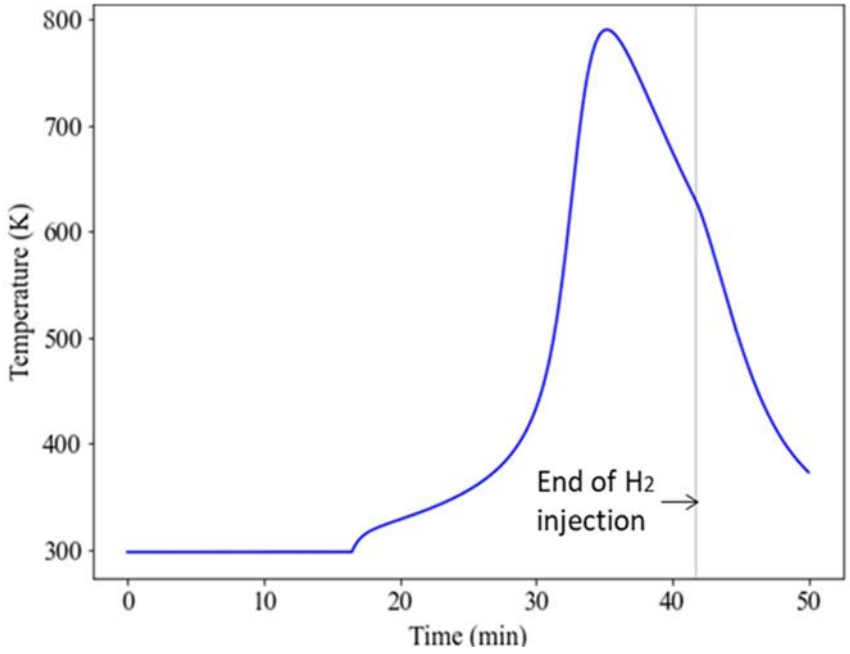

FIG. 44. PAR part-task simulator: catalyst temperature as a function of time in the example of heat transfer coefficient effects (inmost model).

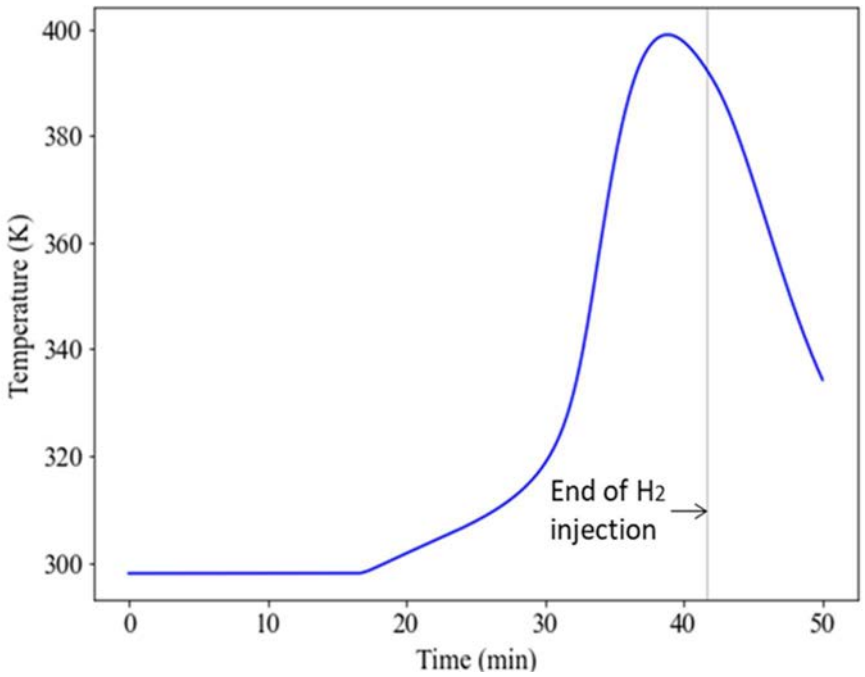

FIG. 45. PAR part-task simulator: gas temperature outside PAR as a function of time in the example of heat transfer coefficient effects (inmost model).

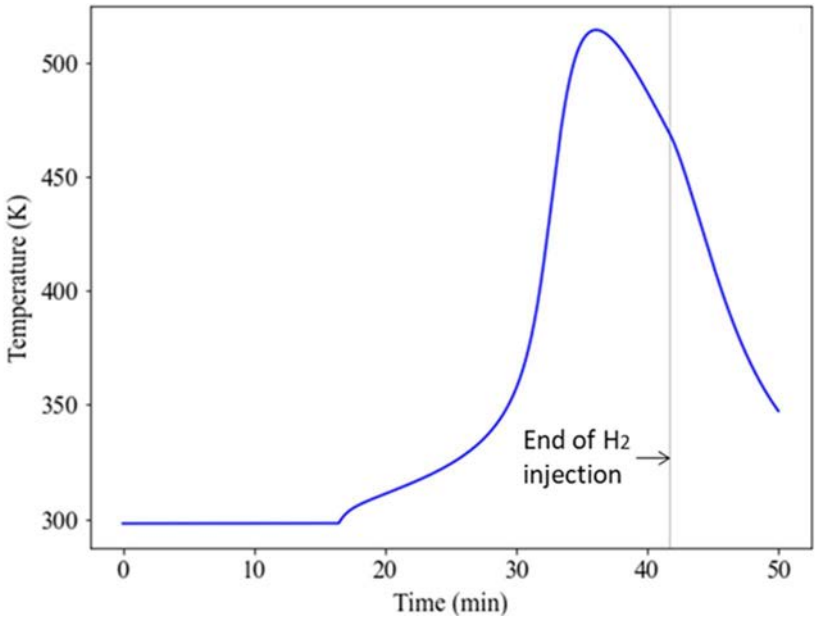

FIG. 46. PAR part-task simulator: gas temperature inside PAR as a function of time in the example of heat transfer coefficient effects (inmost model).

FIG. 47 and FIG. 48 show the time variation of hydrogen concentration outside and inside the PAR, respectively. There is a visible increase in hydrogen concentration outside and inside the PAR because of the decrease in hydrogen depletion rate and the catalyst temperature. The trend is similar as in the example described in Section 4.5.2. The maximum hydrogen concentration outside the PAR is above 3 vol.% whereas the maximum hydrogen concentration inside the PAR is about 2.7 vol.%.

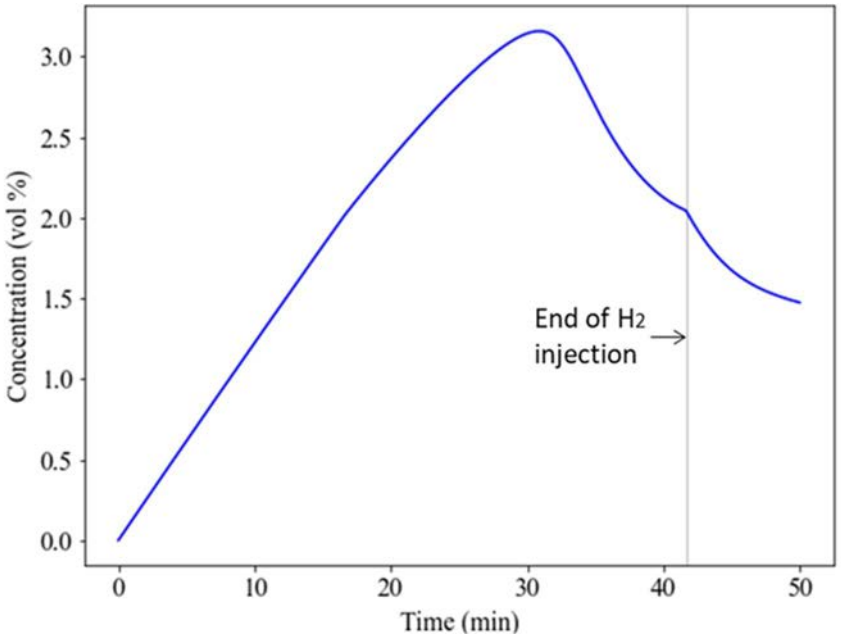

FIG. 47. PAR part-task simulator: hydrogen concentration outside PAR as a function of time in the example of heat transfer coefficient effects (inmost model).

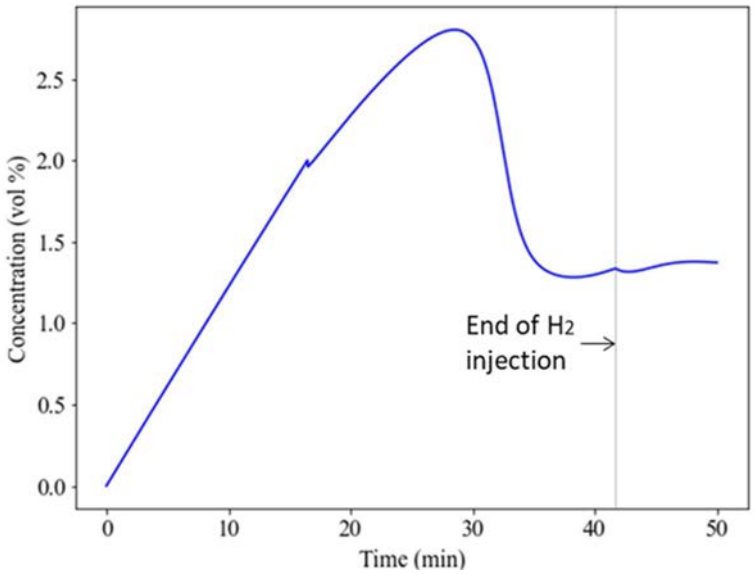

FIG. 48. PAR part-task simulator: hydrogen concentration inside as a function of time in the example of heat transfer coefficient effects (inmost model).

FIG. 49 shows the variation of a single pass efficiency of the PAR at the maximum heat transfer coefficient and the maximum velocity. The single pass efficiency is highly affected by the heat transfer coefficient. It can be seen that the maximum value of the single pass efficiency drops below 50 % as compared to the example described in Section 4.5.2; however, the trend is similar.

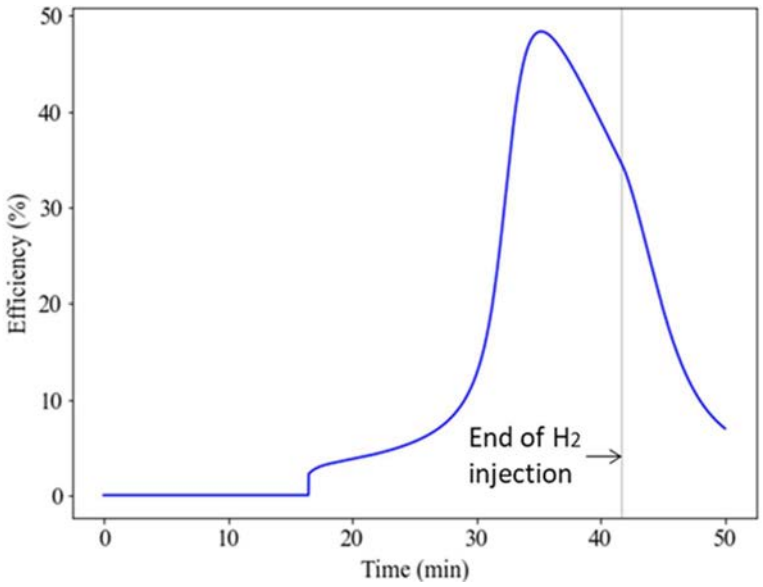

FIG. 49. PAR part-task simulator: single pass efficiency of PAR as a function of time in the example of heat transfer coefficient effects (inmost model).

TABLE 5 provides the peak values of the PAR output parameters as the heat transfer coefficient increases from 0.1 $kWm^{-2}K^{-1}$ to 0.2 $kWm^{-2}K^{-1}$. There is a slight decrease in hydrogen depletion rate initially with increase in heat transfer coefficient and then it increases. The hydrogen concentration inside and outside the PAR and the catalyst temperature affects the hydrogen depletion rate. Thus, the combined effect is a slight increase in hydrogen depletion rate. The

catalyst temperature decreases from 1,028 K to 790 K with increased heat transfer coefficient. Both, hydrogen concentration inside and outside the PAR, increase with increase of heat transfer coefficient whereas the single pass efficiency and the catalyst temperature decreases.

TABLE 5. PEAK VALUES OF THE PAR PARAMETERS AS A FUNCTION OF HEAT TRANSFER COEFFICIENT

Heat transfer coefficient ($kWm^{-2}K^{-1}$)	Hydrogen depletion rate (g/s)	Catalyst temperature (K)	Hydrogen concentration outside the PAR (vol %)	Hydrogen concentration inside the PAR (vol %)	Single pass efficiency (%)
0.10	0.96	1,028	2.5	2.2	61
0.12	0.95	945	2.6	2.3	58
0.14	0.96	889	2.7	2.4	55
0.16	0.97	848	2.9	2.6	52
0.18	0.97	816	3.0	2.7	50
0.20	0.98	790	3.1	2.8	48

5. VALIDATION AND VERIFICATION OF PAR MODELS

5.1. BLACK-BOX MODEL

Given the black-box model is based on conservation of energy for an adiabatic and constant volume space, the calculated after the hydrogen recombination final gas temperature and pressure, are expected to be comparable to theoretical values of adiabatic isochoric complete combustion [7]. Comparison between theoretical values and values obtained using the black-box model of a PAR are summarized in in TABLE 6. The initial hydrogen concentrations are in a range of 8–20 vol.%; the typical operation range for a PAR is well below 8 vol.% hydrogen. The black-box model is applicable only if the initial hydrogen concentration is ≤ 20 vol.%, which covers PAR normal operation range. It can be seen that all calculated values are in a good agreement compared to theoretical values; they are within ± 5% relative error that is defined as follows:

$$\delta[\%] = \frac{|calculated\ value - theoretical\ value|}{theoretica\ \ value} \times 100 \tag{16}$$

TABLE 6. COMPARISON BETWEEN BLACK-BOX MODEL AND THEORETICAL VALUES UNDER THE ADIABATIC ISOCHORIC COMPLETE COMBUSTION CONDITION [7][8]

Initial hydrogen concentration [vol. %]	Initial gas pressure [Pa]		δ [%]	Gas temperature [K]		δ [%]
	Calculated	Theoretical		Calculated	Theoretical	
8	374,130	374,902	0.21	1,142	1,148	0.52
10	431,754	424,199	1.78	1,331	1,312	1.45
12	486,325	476,585	2.04	1,516	1,510	0.40
14	538,486	528,165	1.95	1,696	1,701	0.29
16	588,916	592,751	0.64	1,875	1,895	1.06
18	638,373	628,904	1.51	2,055	2,043	0.59
20	687,807	678,064	1.43	2,239	2,192	2.14

5.2. INMOST MODEL

The two THAI experiments, the hydrogen recombination (HR-) test series, described in [9], [10] are selected to test the inmost model: the HR-3 for the AREVA PAR design and the HR-19 for the AECL PAR design.

The THAI facility consists of a cylindrical vessel with a free volume of ~60 m^3 with different initial atmospheric conditions [11]. The PAR is installed inside the vessel and hydrogen is injected at a controlled rate. The HR-3 test starts with a dry atmosphere, while HR-19 starts with 25 vol.% steam atmosphere. Both tests are performed at an initial pressure of 1.5 bar (152 kPa) [9]. Given that the theoretical model is developed for a generic PAR, the geometrical parameters such as surface area (S_{cata}) and thickness of the catalyst plates are adjusted as they determine the total mass (m_{cata}) of catalyst plates, and the values for v, h_{cata} and c_r. The choice of v is based on the averaged measured values in the HR-19 and HR-3 tests [10]. The values of h_{cata} and c_r shown in TABLE 7, are selected to achieve the observed single-pass efficiency range of 50–70 % [12]. A convergence study with different time steps led to the selection of a 0.01 s time step.

TABLE 7. AECL AND AREVA PAR PARAMETERS USED IN THE INMOST PAR MODEL [8]9]

PAR type	S_{cata} (m^2)	m_{cata} (kg)	v (m/s)	h_{cata} (W/ (m^2 K))	c_r
AECL	2.04	15.70	0.6	200	0.07
AREVA	1.44	1.11	1	60	0.03

The inmost PAR model provides inlet and outlet hydrogen concentrations and gas temperatures, as well as the catalyst temperature as a function of time. These are compared to the THAI experimental values for the AECL and AREVA PARs [8]. The inlet and outlet hydrogen concentrations are assumed to be equal to the homogeneous outside and inside PAR hydrogen concentrations, respectively. The adapted parameters shown in TABLE 7 are not constant but they change as PAR operates.

FIG. 50 (*a*) shows the catalyst temperature change with time. It can be seen that the agreement between calculated and experimental values is realistic. The maximum calculated catalyst plate temperature agrees with the experimental maximum temperature within 50 °C. In the real environment, velocity and heat transfer coefficients are low at PAR start-up because of the temperature difference between the catalyst plates and the inside gas being small. This makes the catalyst to heat up quickly. The increased catalyst temperature increases the velocity and heat transfer coefficients, which in turns slows down the heating of the catalyst. Similar discrepancy is observed during the cooling of catalyst plates.

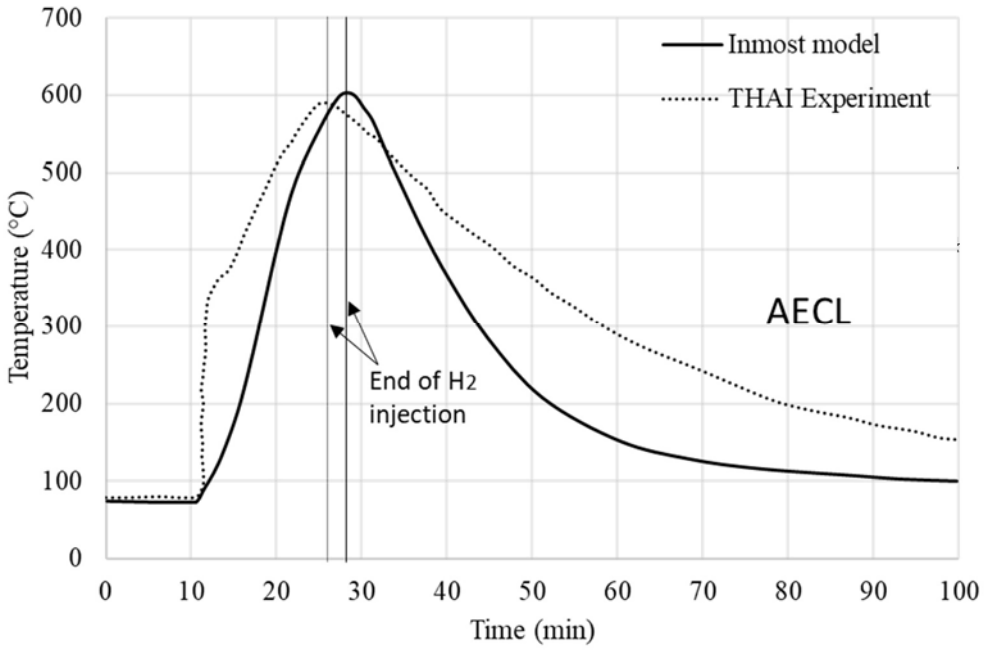

(a)

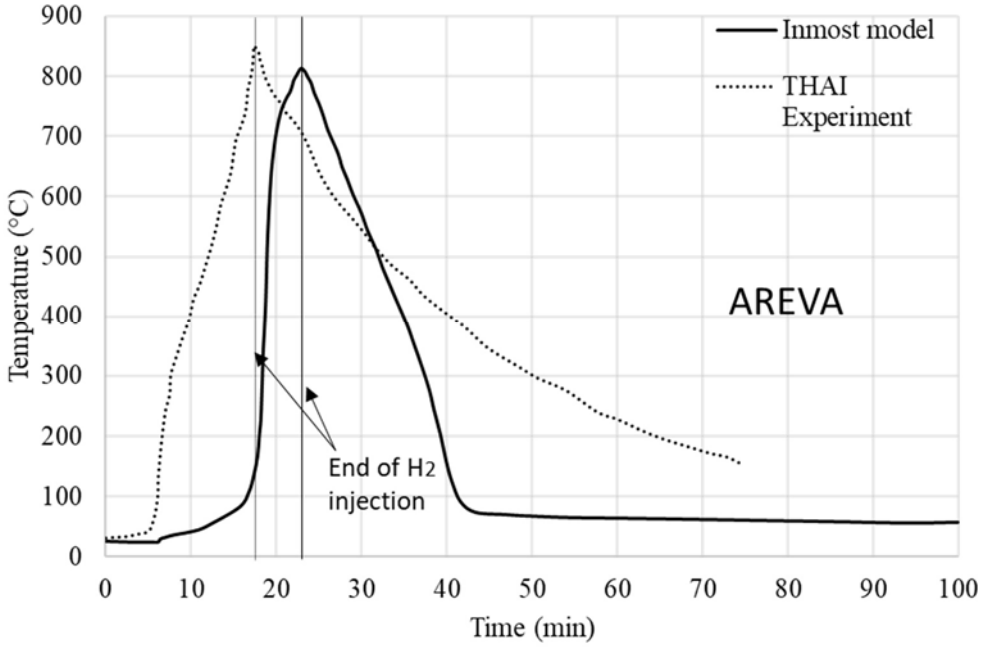

(b)

FIG. 50. Comparison of catalyst temperature as a function of time between the inmost PAR model and THAI experimental values: (a) comparison to AECL PAR, (b) comparison to AREVA PAR.

FIG. 51 (*a*) and *(b)* show calculated inlet hydrogen concentration change with time in comparison to THAI experiments for AECL and AREVA PAR. It can be seen that the inmost PAR model reproduces almost the same results as the AECL PAR. It deviates largely from the AREVA PAR after the end of hydrogen injection as natural circulation is neglected in inmost PAR model.

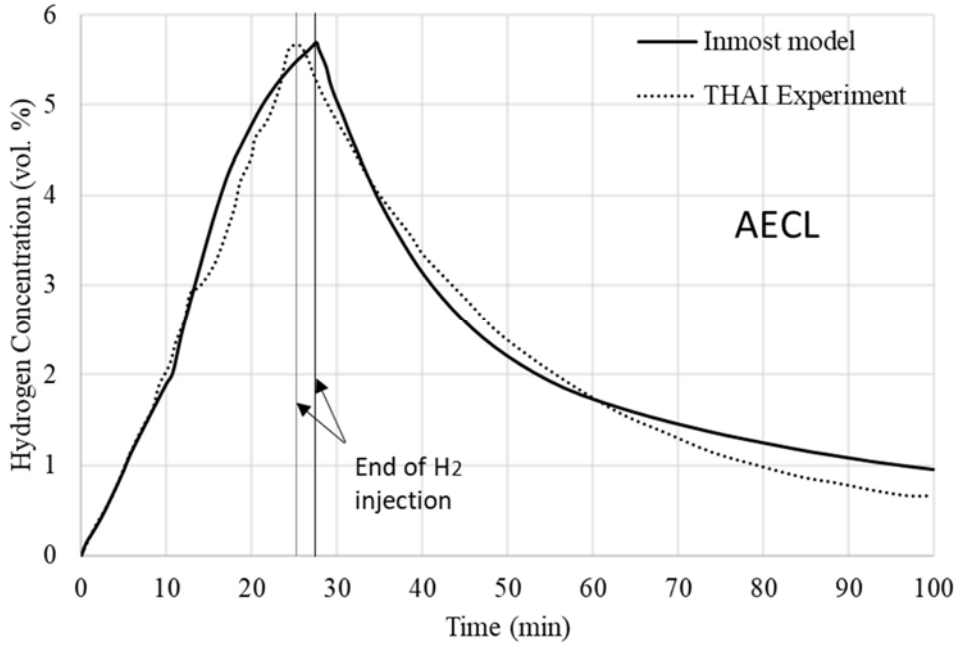

(a)

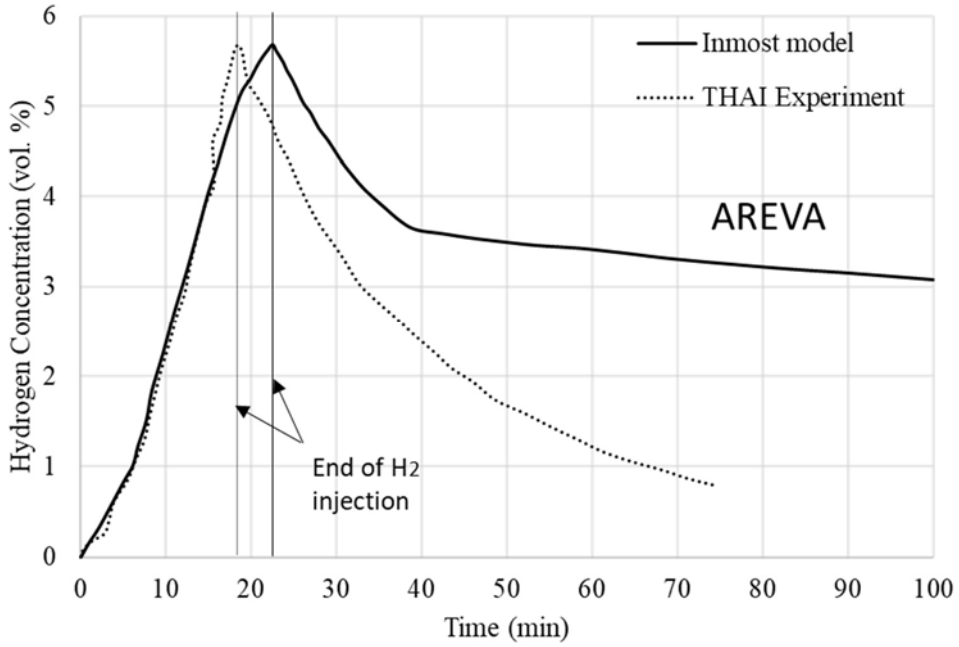

(b)

FIG. 51. Comparison of inlet hydrogen concentration between the inmost PAR model and THAI experimental values: (a) AECL PAR, (b) AREVA PAR.

FIG. *52* (*a*) shows time dependence of the outlet hydrogen concentrations. The values vary quite significantly right after the PAR start-up. It is attributed to the assumptions introduced in the inmost PAR model unable to capture the actual transients within the PAR (simplified recombination without considering diffusion kinetics of the gas inside the PAR, which plays an important role in the recombination process itself [13]). The model provides comparable results

for the evolution of catalyst temperature and outside PAR hydrogen concentration, which is of prime importance for a PAR part-task educational simulator. FIG. *52* (*b*) again shows the discrepancy between calculated and experimental values for the AREVA PAR in comparison to the AECL PAR.

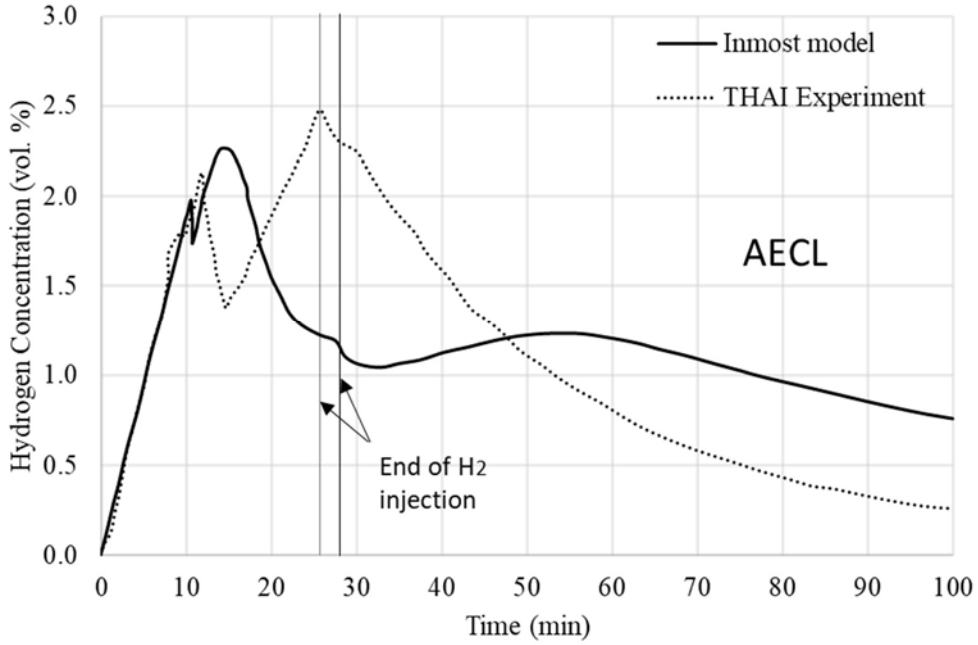

(a)

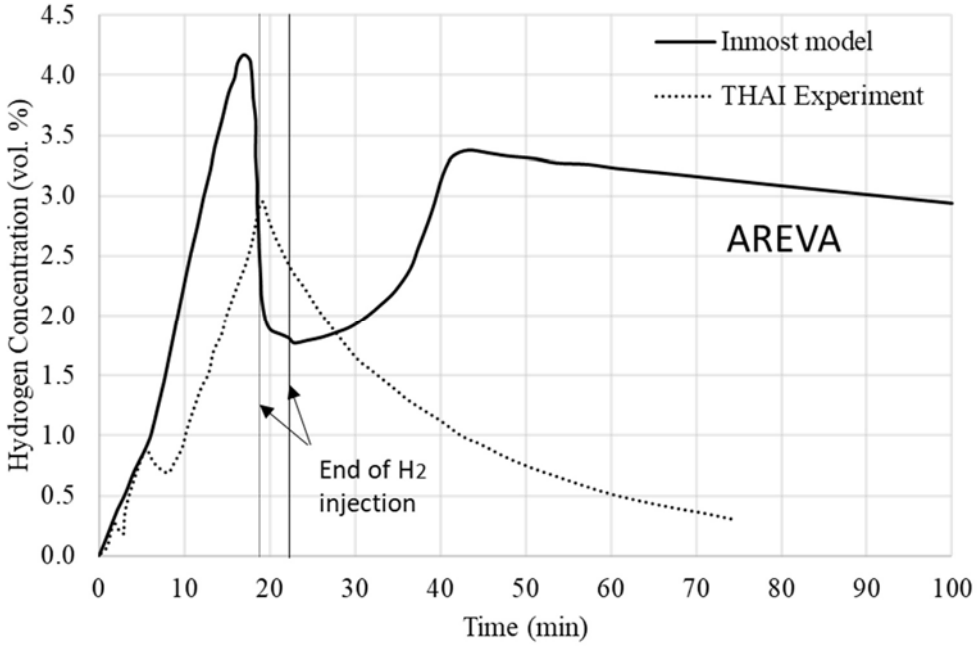

(b)

FIG. 52. Comparison of outlet hydrogen concentration as a function of time between the inmost PAR model and THAI experimental values[8].

REFERENCES

[1] INTERNATIONAL ATOMIC ENERGY AGENCY, Classification, Selection and Use of Nuclear Power Plant Simulators for Education and Training, IAEA-TECDOC-1887, IAEA, Vienna (2019).

[2] INTERNATIONAL ATOMIC ENERGY AGENCY, Development in the Analysis and Management of Combustible Gases in Severe Accidents in Water Cooled Reactors following the Fukushima Daiichi Accident, IAEA-TECDOC-1939, IAEA, Vienna (2020).

[3] INTERNATIONAL ATOMIC ENERGY AGENCY, Hydrogen Phenomenon during Severe Accidents in Water Cooled Reactors, IAEA-TCS-72, IAEA, Vienna (2021).

[4] SCHEFER, R.W., Catalyzed combustion of H2/air mixtures in a flat plate boundary layer: II. Numerical model, Combustion and Flame **45** (1982) 171, 190.

[5] CENGEL, Y.A., BOLES, M. A., Thermodynamics: An Engineering Approach, McGraww-Hill, New York (2007), 887 pp.

[6] ROZEN, A., Modelling of a passive autocatalytic hydrogen recombiner: a parametric study, Nukleonika **60** 1 (2015) 161, 169.

[7] LAUTKASKI, R., Pressure Rise in Confined Gas Explosions, VVT Processes, Nuclear Energy, Finland (2005).

[8] LIANG, D., KALEEM, M. A., et. al., The International Atomic Energy Agency Part-Task Simulator on Passive Autocatalytic Recombiners, The 19th International Topical Meeting on Nuclear Reactor Thermal Hydraulics, NURETH-19, Brussels, Belgium (2022).

[9] KAZLEITER, T., et al., OECD/NEA THAI Project Hydrogen and Fission Porduct Issues Relevant for Containment Safety Assessment Under Severe Accident Conditions, NEA/CSNI, France (2010).

[10] REINECKE, E. A., et al., Validation and application of the REKO-DIREKT code for the simulation of passive autocatalytic recombiner operational behavior, Nuclear Technology **196** 2 (2016) 355, 366.

[11] INTERNATIONAL ATOMIC ENERGY AGENCY, Simulation and Experimental Network Information On-line System, SANIS database, Pages - SANIS (iaea.org).

[12] GUPTA, S., et al., Main Outcomes and Lessons Learned from THAI Passive Autocatalytic Recombiner Experimental Research and Related Model Development Work, in 17th International Topical Meeting on Nuclear Reactor Thermal Hydraulics (NURETH-17), Xi'an, China (2017).

[13] ROZEN, A., Simulation of start-up behaviour of a passive autocatalytic hydrogen recombiner, Nukleonika **63** 2 (2018) 27, 41.

ABBREVIATIONS

AECL	Atomic Energy of Canada Limited
AREVA	Industrial group active in nuclear fuel cycle and construction of nuclear installations
NPP	Nuclear Power Plant
PAR	Passive Autocatalytic Recombiner
THAI	Thermal hydraulics, Hydrogen, Aerosols, and Iodine Experimental Facility

CONTRIBUTORS TO DRAFTING AND REVIEW

Jevremovic, T.	International Atomic Energy Agency
Kaleem, M. A.	Pakistan Institute of Engineering and Applied Sciences, Pakistan
Krause, M.	International Atomic Energy Agency
Liang, D.	International Atomic Energy Agency
Rehman, H ur.	International Atomic Energy Agency
Riaz, W.	International Atomic Energy Agency
Sungur, N.	International Atomic Energy Agency

IAEA
International Atomic Energy Agency

No. 26

ORDERING LOCALLY

IAEA priced publications may be purchased from the sources listed below or from major local booksellers.

Orders for unpriced publications should be made directly to the IAEA. The contact details are given at the end of this list.

NORTH AMERICA

Bernan / Rowman & Littlefield

15250 NBN Way, Blue Ridge Summit, PA 17214, USA
Telephone: +1 800 462 6420 • Fax: +1 800 338 4550

Email: orders@rowman.com • Web site: www.rowman.com/bernan

REST OF WORLD

Please contact your preferred local supplier, or our lead distributor:

Eurospan Group

Gray's Inn House
127 Clerkenwell Road
London EC1R 5DB
United Kingdom

Trade orders and enquiries:

Telephone: +44 (0)176 760 4972 • Fax: +44 (0)176 760 1640
Email: eurospan@turpin-distribution.com

Individual orders:

www.eurospanbookstore.com/iaea

For further information:

Telephone: +44 (0)207 240 0856 • Fax: +44 (0)207 379 0609
Email: info@eurospangroup.com • Web site: www.eurospangroup.com

Orders for both priced and unpriced publications may be addressed directly to:

Marketing and Sales Unit
International Atomic Energy Agency
Vienna International Centre, PO Box 100, 1400 Vienna, Austria
Telephone: +43 1 2600 22529 or 22530 • Fax: +43 1 26007 22529
Email: sales.publications@iaea.org • Web site: www.iaea.org/publications

23-03177E

INTERNATIONAL ATOMIC ENERGY AGENCY
VIENNA